Global and Planetary Change 194 (2020) 103291

Contents lists available at ScienceDirect

Global and Planetary Change

journal homepage: www.elsevier.com/locate/gloplacha

Mercury anomalies and carbon isotope excursions in the western Tethyan Csővár section support the link between CAMP volcanism and the end-Triassic extinction

Emma Blanka Kovács[a,b,c,d,*], Micha Ruhl[c,d,e], Attila Demény[f], István Fórizs[f], István Hegyi[f], Zsófia Rita Horváth-Kostka[a], Ferenc Móricz[g], Zsolt Vallner[a,b], József Pálfy[a,h]

[a] Department of Geology, Eötvös Loránd University, Pázmány Péter sétány 1/C, Budapest H-1117, Hungary
[b] Isotope Climatology and Environmental Research Centre (ICER), Institute for Nuclear Research, Bem tér 18/C, Debrecen H-4026, Hungary
[c] Department of Geology, Trinity College Dublin, The University of Dublin, College Green, Dublin 2, Ireland
[d] Earth Surface Research Laboratory (ESRL), Trinity College Dublin, The University of Dublin, Dublin 2, Dublin, Ireland
[e] Irish Centre for Research in Applied Geosciences (iCRAG), Trinity College Dublin, The University of Dublin, College Green, Dublin 2, Dublin, Ireland
[f] Institute for Geological and Geochemical Research, Research Centre for Astronomy and Earth Sciences (RCAES), Budaörsi út 45, Budapest H-1112, Hungary
[g] Institute of Mineralogy and Petrology, University of Miskolc, Miskolc-Egyetemváros H-3515, Hungary
[h] MTA–MTM–ELTE Research Group for Paleontology, Pázmány Péter sétány 1/C, Budapest H-1117, Hungary

ARTICLE INFO

Keywords:
Triassic–Jurassic boundary
stable carbon isotopes
mercury
chemostratigraphy
CAMP large igneous province

ABSTRACT

The end-Triassic extinction is one of the major Phanerozoic mass extinctions and it appears to have been linked to coeval rapid and severe environmental change, thought to be triggered by volcanism in the Central Atlantic Magmatic Province (CAMP). However, direct stratigraphic evidence to substantiate this linkage and to help develop scenarios for the cascade of events is still scarce. Mercury is an increasingly widely used proxy to trace the volcanic activity associated with large igneous provinces (LIPs) in distal sedimentary sections, but so far Hg records are available from only a handful of Triassic–Jurassic boundary (TJB) sections. One of the few well-studied marine sedimentary sections with a continuous sedimentary record across the TJB is located at Csővár (Hungary) and it exposes an extended succession of carbonates deposited in an intraplatform basin on the western Tethyan shelf. Previously, this section yielded one of the first convincing records of carbon isotope excursions (CIEs) across the TJB, albeit from low-resolution sampling. Here we report a new, high-resolution $\delta^{13}C_{carb}$ curve, supplemented with Hg measurements. A series of successive negative carbon isotope excursions (termed NCIE-1 to 6) attests to carbon cycle perturbations in the TJB interval. Four excursions appear significant after statistical smoothing. Of these, NCIE-3 exhibits the highest amplitude and is biostratigraphically constrained to the topmost Triassic, hence reliably correlated with the *initial* CIE, a globally recognised excursion closely preceding the TJB, and coincident with the end-Triassic extinction (ETE) horizon. The Hg concentration data provide the longest record available to date from a single section across the TJB. It shows very low values below NCIE-3 that are interpreted as the pre-volcanic background, followed by a prominent Hg peak that is nearly coincident with the most significant carbon isotope spike (NCIE-3). The slight lag suggests that onset of a major extrusive phase of CAMP (marked by a significant rise in Hg) closely followed the very onset of carbon cycle perturbation at that time (expressed by an abrupt change in the $\delta^{13}C_{carb}$ signal), possibly from biogenic methane release. Subsequent and recurring smaller Hg psuggest a pulsatory nature of prolonged volcanic activity. Organic content in the section is consistently low and sedimentary Hg concentrations are therefore normalized against Fe content, a reliable proxy in the lack of significant lithological changes. The maximum sedimentary Hg concentration at Csővár is greater than that in any other TJB section, although not unprecedented if other events are considered. Three hypotheses are explored to explain the high values; i) the hit-or-miss model could suggest that deposition of the sampled beds was fortuitously coincident with major eruptions, ii) the presence and preservation of cryptotephra could account for the unusually high sedimentary Hg enrichment, and iii) changes in the proportion of Hg-carrier phases throughout the studied succession, e.g. from magnetite to pyrite dominance, could have enhanced the potential of Hg capture and deposition. Collectively, the new data provide direct stratigraphic and geochemical evidence for the link between CAMP volcanism and carbon cycle perturbations and strengthen the case of their causal relationship with the end-Triassic extinction.

* Corresponding author.
E-mail address: kovacse@tcd.ie (E.B. Kovács).

https://doi.org/10.1016/j.gloplacha.2020.103291
Received 16 April 2020; Received in revised form 31 July 2020; Accepted 3 August 2020
Available online 14 August 2020

1. Introduction

Large igneous provinces (LIPs) were commonly synchronous with, and are suspected to be the main trigger of, cascades of environmental changes and concomitant mass extinctions that fundamentally influenced the Phanerozoic history of the Earth system (Wignall, 2005; Bond et al., 2014). LIP-related greenhouse gas emissions and attendant global warming, ocean acidification and anoxia are key components of scenarios proposed to explain observational evidence from the stratigraphic and fossil records (Bond and Grasby, 2017); therefore inferences from past events may inform predictions of trajectories of global change from greenhouse gas forcing in the Anthropocene (Waters et al., 2016). The end-Triassic mass extinction (ETE) and its relation to the Central Atlantic Magmatic Province (CAMP) has been a prominent example and the subject of several case studies exploring the LIP-extinction linkage (e.g. Marzoli et al., 1999; McElwain et al., 1999; Pálfy, 2003; Whiteside et al., 2007; Pálfy and Zajzon, 2012; Jaraula et al., 2013; Pálfy and Kocsis, 2014; Thibodeau et al., 2016; Percival et al., 2017; Heimdal et al., 2018).

The temporal coincidence of the age of CAMP volcanics and marine and terrestrial biotic extinctions (Marzoli et al., 1999; Pálfy et al., 2000) contributed to establishing the overall pattern of synchrony of LIPs and extinction events (Courtillot and Renne, 2003). The subsequent realization that complex and intertwined environmental and biotic changes are best reflected in perturbations of the carbon cycle, was evidenced by discoveries of major negative carbon isotope excursions (NCIEs) across the Triassic–Jurassic boundary (TJB) interval (Pálfy et al., 2001; Ward et al., 2001; Hesselbo et al., 2002). In the past two decades a multitude of studies documented carbon isotope excursions (CIEs) around the TJB and used them either for stratigraphic correlation or reconstruction of changes in carbon cycle dynamics or both (Korte et al., 2019). However, controversies exist, and alternative interpretations have been proposed as causes for the CIEs, especially concerning the immediate cause for the CIE correlated with the ETE-horizon, on whether subsurface intrusion-related gas release, explosive-magmatic gas release, or enhanced biogenic methane gas release was more potent (Beerling and Berner, 2002; Ruhl et al., 2010a, 2010b; Ruhl and Kürschner, 2011; Davies et al., 2017; Capriolo et al., 2020). Clearly, new high-resolution records of biostratigraphically constrained TJB sections are needed to help resolve these issues.

Beyond establishing the temporal link of CAMP volcanism and the ETE, and the plausible role of LIP-driven environmental changes in triggering the biotic crisis, significant effort went into finding direct markers of volcanism in marine sedimentary sections where the extinction event is best documented. Mafic mineral grains supposedly from air-fallen ash, distinctive clay minerals thought to derive from alteration of basaltic volcanic glass, and anomalous enrichment of rare earth elements (REE) at the TJB in a western Tethyan marine section now exposed in the Northern Calcareous Alps was proposed as distal evidence for coeval CAMP activity (Pálfy and Zajzon, 2012; Zajzon et al., 2012). In recent years, mercury-concentration and Hg/TOC (Hg data normalized against the total organic carbon content) data have been increasingly used, and proved as a possibly useful geochemical tracer of distal volcanic activity in sedimentary sections (Grasby et al., 2019 and references therein). This new proxy has been tested in only a few studies in a limited number of TJB sections (Thibodeau et al., 2016; Percival et al., 2017; Lindström et al., 2019; Ruhl et al., 2020). Although these results are promising, they are somewhat controversial, due to potential issues in stratigraphic correlation between sections and the lack of understanding of processes that control the variability in Hg-enrichment in different sediments and between different sites. Combined, these issues underscore the need for the stratigraphic study of a sedimentary succession marked by non-variable marine depositional conditions.

To augment the available database and advance our understanding on potential CAMP-ETE causal links, here we present and integrate new high-resolution Hg-concentration and $\delta^{13}C_{carb}$ records from Csővár, a key TJB section with a rich history of recent studies (Pálfy and Dosztály, 2000; Pálfy et al., 2001, 2007; Götz et al., 2009; Haas et al., 2010). The Csővár section in Hungary shares some similarities in paleogeographic and depositional setting with other western Tethyan reference sections in the Northern Calcareous Alps in Austria, including the GSSP for the base of the Jurassic system at Kuhjoch (Hillebrandt et al., 2013). Although the Csővár section was one of the first localities where the prominent NCIE at the ETE was documented (Pálfy et al., 2001) and confirmed by further studies (Pálfy et al., 2007), the data resolution was inadequate by current standards, and correlation of the set of CIEs to other localities remained contentious, requiring the generation of new data from denser sampling, which is reported here. In contrast to most other sections, the lack of significant lithological changes at Csővár, combined with a relatively elevated sedimentation rate provides an opportunity to obtain Hg concentration data at a higher temporal resolution than in previously studied sections. As we report a series of Hg and $\delta^{13}C_{carb}$ anomalies over the extended TJB interval, we integrate the previously studied records from other TJB sections to assess whether the Hg load was indeed sourced by CAMP and discuss possible mechanisms of formation and preservation of the Hg signal. Our results add to the ongoing debate about the characteristics and reliability of the Hg proxy for LIP volcanism and help refine scenarios of carbon cycle changes and biotic extinction across the TJB.

2. Background

2.1. Carbon isotope excursions

The Triassic–Jurassic transition is marked by dramatic global biotic turnover, known as the end-Triassic extinction. Near the extinction horizon, there is a significant NCIE, observed in marine and terrestrial sedimentary archives, across both hemispheres, which suggests a major perturbation of the carbon cycle. This anomaly is widely used as a global correlation tool, commonly referred to as the *initial* CIE (*e.g.* Pálfy et al., 2001; Ward et al., 2001; Hesselbo et al., 2002). There are other anomalies around the boundary, such as the *precursor* CIE and the *main* CIE, however, their global significance remains debated (*e.g.* Hesselbo et al., 2002; Ruhl et al., 2009; Ruhl et al., 2010a; Ruhl and Kürschner, 2011). An alternative naming and correlation scheme of CIEs was poposed recently, based on a combination of palynostratigraphy and ammonite biostratigraphy (Lindström et al., 2017). Their emphasis on the use of palynological data, obtained from marine sedimentary successions, led to discrepancies with the ammonite records as taxon ranges and abundance distribution of palynomorphs are sensitive to paleoenvironmental differences and thus vary geographically and between sections. An additional nomenclatural issue concerns the use of Spelae Zone, which is no longer an accepted zone and is thus not a biostratigraphic unit, therefore the younger two CIEs both belong to the Tilmanni Zone. Due to these controversies, we use the more widely established correlation scheme as advocated by Korte et al. (2019).

2.2. Mercury anomalies as proxy for LIP volcanism

Large Igneous Province volcanism and mass extinctions often occur synchronously (Bond et al., 2014), however, their cause-and-effect relationship is not uniformly accepted (e.g. Grasby et al., 2019; Schoene et al., 2019). Volcanogenically induced elevated carbon fluxes (e.g. from basalt degassing, thermogenic and biogenic methane release) may have impacted on the global carbon cycle, but its stratigraphic link to the onset or peak of magmatism is poorly constrained, and carbon release as cause for mass extinction cannot be convincingly demonstrated in every case (Self et al., 2006, 2014). In addition, not every LIP has a matching extinction and vice versa (Wignall, 2001).

A recently developed proxy to establish a potential link between past extinctions, as recorded in sedimentary archives, and LIP activity

utilizes elevated levels of sedimentary Hg as an indicator of major volcanism (Sanei et al., 2012). Modern day volcanism increases significantly the atmospheric Hg concentration, implying that LIP activity would potentially release large amounts of Hg into the atmosphere (Grasby et al., 2019 and references therein), e.g. ~3800 Mt of extra Hg is connected to the emplacement of the Siberian Traps (Wang et al., 2019) and ~150 Mt of Hg to emplacement of the Karoo-Ferrar LIP (Grasby et al., 2019). Mercury release from LIP emplacement possibly largely results from volcanogenic degassing, but it can also be released during the intrusive phase and resulting contact metamorphism with organic-rich sediments (Grasby et al., 2013; Percival et al., 2015; Heimdal et al., 2019; Jones et al., 2019).

The present-day natural Hg cycle is marked by multiple sources and sinks, as well as temporary Hg reservoirs (Fig. 1). The most important natural source of Hg in modern environments is the direct emission from volcanism, on land and in the oceans. In the present-day ocean Hg-concentrations vary significantly, between 1×10^{-5}–2.4×10^{-4} ppb, largely depending on the proximity to mid-ocean ridges, as its residence time is around 350 years (Gill and Fitzgerald, 1988; Bowman et al., 2015).

The dominant phase of Hg released into the atmosphere, from terrestrial volcanism, occurs in the form of elemental gas (Hg^0) and its atmospheric residence time is 0.5–1.5 yr (Pyle and Mather, 2003; Selin, 2009; Wang et al., 2019), allowing for a global distribution in the present-day atmosphere (Schroeder and Munthe, 1998). Hg^{+2} is the more common oxidation state (+1 is rarer), which can also be transported aerially; however, Hg^{+2} will be transported across much shorter distances (in the order of 10–100 km), as it stays in the atmosphere for only a few weeks (Schroeder and Munthe, 1998; Grasby et al., 2019). Solid-state Hg can be volcanogenically emitted, and the distance between source and deposition depends largely on the diameter and/or mass of the aerosol particle that Hg_s may be attached to (Schroeder and Munthe, 1998). During explosive volcanic activity, marked by extremely high plumes (20–40 km in altitude, reaching the more stable stratosphere), gaseous and ash-bound Hg may be able to travel large distances, carried by stratospheric winds (Grasby et al., 2019).

Deposition of Hg, i.e. its removal from the atmosphere, depends on the concentration of the different Hg phases. If the concentration of Hg^{+2} and/or Hg_s is greater than 100 pg/m^3 then Hg can be removed through wet and dry deposition (Holmes et al., 2010; Grasby et al., 2019). However, if these Hg-phases have lower concentrations in the atmosphere, then Hg is removed by wet deposition and oxidation of Hg^0. Although Holmes et al. (2010) suggest that bromine can also oxidize Hg^0, HgO_g is commonly the product of reactions with O_3, NO_3 or other oxides (Hall, 1995). The newly formed HgO_g is then adsorbed by aerosol particles, which are removed from the atmosphere through precipitation (Poissant, 1997).

Plants aid in the dry removal of Hg from the atmosphere as Hg is adsorbed onto leafs and either taken up by the stomata or washed off by precipitation into the soil (Schroeder and Munthe, 1998). The amount of Hg in plant tissue is closely related to the atmospheric Hg concentration (Grasby et al., 2019), but varies significantly between plant-species due to different adsorption rates. If Hg is taken up and retained by plants, it can enter the soil with the litterfall, after which it can be re-mobilized and taken up by the root system (Schroeder and Munthe, 1998). As plants can be enriched in Hg, elevated wildfire activity can enhance the Hg-flux into the atmosphere. For example, it has been proposed that an increased wildfire activity in the latest Permian, in response to Siberian Traps emplacement driven climatic and environmental change, resulted in an elevated flux of Hg into the ocean-atmosphere system (Grasby et al., 2017).

Other natural Hg sources into past environments may have been the melting of permafrost, or continental weathering (de Lacerda et al., 2017; Grasby et al., 2019). Whatever the source of Hg, as reactive Hg^{2+} reaches the ocean, it commonly forms MeHg (methylmercury), which then accumulates and builds Hg-OM (organo-mercury complexes) (Ravichandran, 2004).

The analyses of changes in the Hg abundance in sedimentary archives spanning major global change events and/or large igneous province emplacement, potentially allows for constrains on the change in Hg capture and storage compared to the average Hg influx over geological time (Grasby et al., 2019). Due to the reactivity of the Hg, there is likely no long-term Hg accumulation in the marine reservoir.

As Hg is most often attached to organic matter, usually the TOC and Hg concentration curves in sedimentary archives evolve parallel to one another, because changes in the sedimentary Hg concentration are resulting from changes in its sequestration with organic matter, rather than in Hg loading of the environment (Outridge et al., 2007; Gehrke et al., 2009; Sanei et al., 2012). For this reason, sedimentary Hg-concentrations are commonly normalized against TOC and reported as Hg/TOC values. However, due to the increasing uncertainty on TOC analyses in low TOC samples, normalization should be avoided when TOC < 0.2 wt%; and even with TOC values below 0.5 wt% caution must be taken (Grasby et al., 2019).

Although Hg is commonly bound to organic matter, it can also occur in a bond to clay minerals, or as sulphides (such as pyrite (FeS_2), pyrrhotite ($Fe_{1-x}S$) and mackinawite (FeS); under anoxic depositional conditions), or in Fe-oxides (under oxic depositional conditions) (Shen et al., 2019a, 2020 and references therein). It may therefore be useful (or essential) to normalize sedimentary Hg concentrations against Al, Fe, and/or total/pyrite S (Grasby et al., 2019).

3. Geological and stratigraphic background

The Vár-hegy section near the village of Csővár lies 50 km north-northeast of Budapest (Fig. 2), within the fault-bounded Nézsa-Csővár block on the left side of the Danube, at the northeastern extremity of the Transdanubian Range, within the Alcapa Megaunit (Csontos and Vörös, 2004). Palaeogeographically, it formed part of an intraplatform basin near the external margin of the extensive Dachstein carbonate platform system that started to disintegrate in the Late Triassic–Early Jurassic, due to the ongoing opening of the Neotethys Ocean (Fig. 3) (Haas et al., 2010, 2012). The Nézsa-Csővár block consists of Triassic–Jurassic and Eocene sedimentary rocks. The Mesozoic carbonates were deposited on the slope and in the basin, as well as on the adjacent platform; slope and

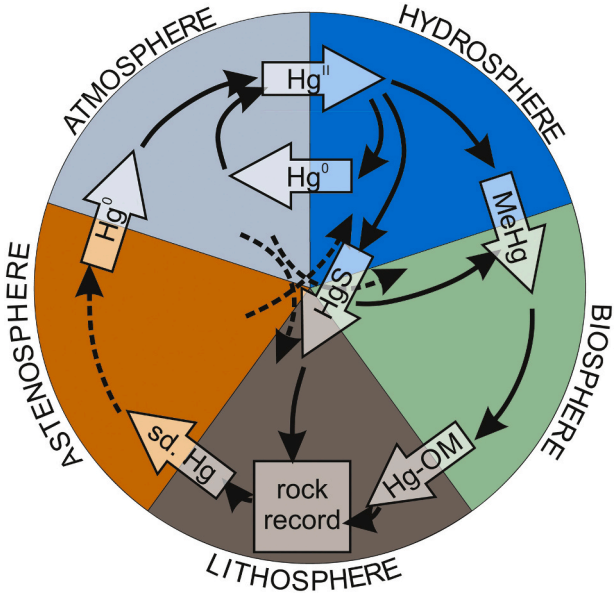

Fig. 1. The natural Hg cycle. The wide-open arrows show the dominant phase in which Hg is transported, whereas the black arrows represent the possible transition pathways between Hg phases (with solid lines for known and dashed lines for assumed but less explored pathways).

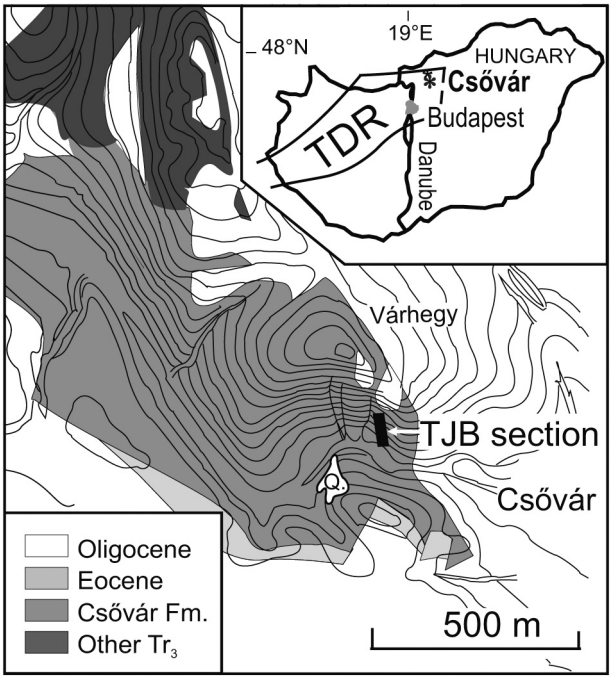

Fig. 2. Geographical location and geological context of the studied section.TDR: Transdanubian Range, TJB: TriassicJurassic boundary. From Pálfy et al. (2001).

basinal facies are assigned to the Csővár Limestone Formation. The lower (Upper Carnian–Lower Rhaetian) part of the Csővár Limestone Formation was penetrated by the Csv-1 core. Higher parts of the formation are exposed in the Pokol-völgy quarry (Haas et al., 1997) and on the south-facing, steep slope of the Vár-hegy. The latter outcrop includes the Rhaetian–Hettangian interval (Pálfy and Dosztály, 2000) and extends up to the Sinemurian (Kozur, 1993). The Csővár area is structurally complex as it was affected by Late Cretaceous–Early Paleogene folding, and subsequently segmented by younger normal faults (Benkő and Fodor, 2002). The measured TJB section lies within a stratigraphically intact domain with gently northeast-dipping strata.

The Vár-hegy section has been known for over 150 years (Szabó, 1860); its significance as a continuous TJB section was only recognized much later, with the boundary identified at around 20 m (Pálfy and Dosztály, 2000). Detailed microfacies studies revealed remarkable lithological continuity between the Triassic and Jurassic parts of the succession (Haas and Tardy-Filácz, 2004). The first 11 m of the section (Fig. 4) consists of laminated calcareous mudstone alternating with thin to medium-bedded limestone, followed by a 1 m thick bioclastic limestone bed. In the interval of 12–15 m laminated calcareous mudstone is the most common rock type. From there, up to 32 m, slumps are common features in the sequence. Between 32–34 m, platform-derived ooidal limestone is exposed. The upper part of the 57 m thick measured section comprises laminated calcareous mudstone alternating with bedded limestone and limestone with slumps (Pálfy and Dosztály, 2000). The sedimentary succession at Csővár is consistent with its origin at the foreslope of a carbonate platform and in proximal to distal parts of an intraplatform basin. Microfacies analyses suggest a general upward deepening trend that can be considered as the record of the transgressive phase of a long-term, second order transgression-regression cycle. Meter-scale cyclicity is observed in the alternation of calcareous turbidite and basinal facies, which may be interpreted as third- and fourth order cycles (Haas and Tardy-Filácz, 2004).

3.1. Ammonoid biostratigraphy

The position of the TJB is approximated by several fossil groups, but each group has a sporadic record due to preservation issues. Despite intensive sampling efforts, the last occurrence of various Triassic and the first occurrence of Jurassic taxa are congruent albeit recorded at different levels. Ammonoids are of paramount importance as they provide the primary marker for the TJB definition (Hillebrandt et al., 2013). Ammonoids are rare in the section and are poorly or moderately

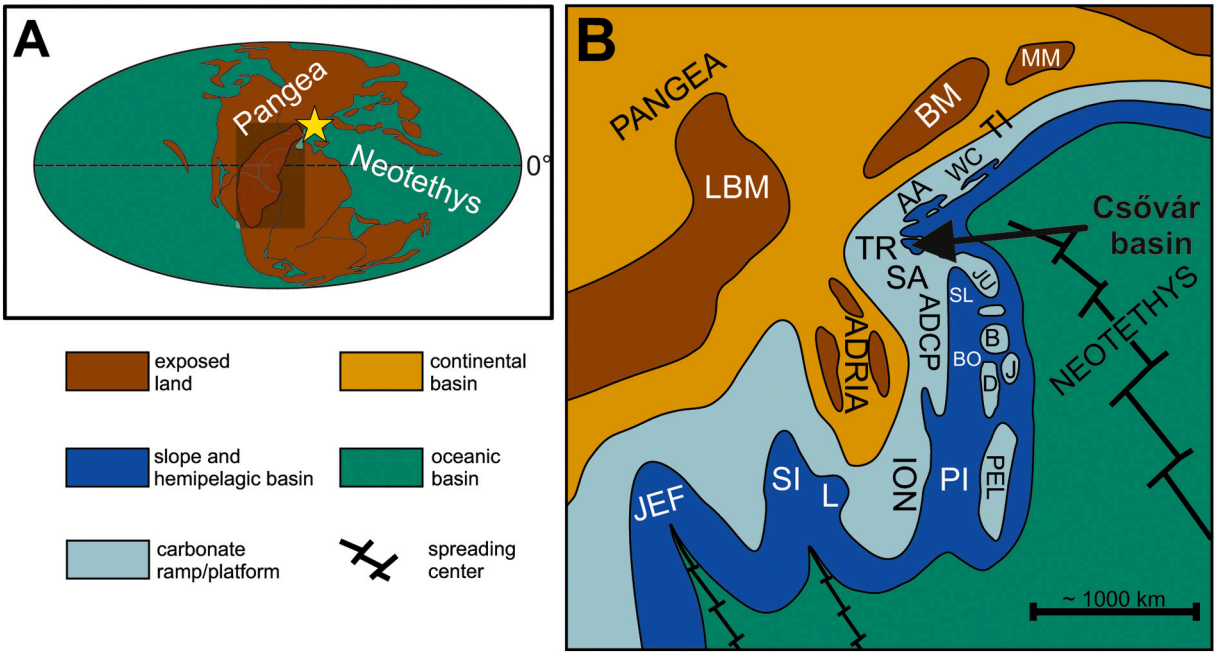

Fig. 3. Palaeogeographical position of the Csővár basin in global context (panel A) and within the western Neotethys (panel B). CAMP: Central Atlantic Magmatic Province, LBM: London-Brabant Massif, BM: Bohemian Massif, MM: Malopolska Massif, AA: Austroalpine Units, WC: Central and Inner West Carpathian Units, TI: Tisza Unit, TR: Transdanubian Range, SL: Slovenian basin, JU: Julian Alps, B: Bükk Unit, ADCP: Adriatic-Dinaridic Carbonate Platform, BO: Bosnian Zone, D: Drina–Ivanjica Unit, J: Jadar Block, SI: Sicilian Basin, L: Lagonegro Basin, JEF: Jefra Basin, PI: Pindos Basin, PEL: Pelagonian-Subpelagonian Units. After Haas et al. (2019).

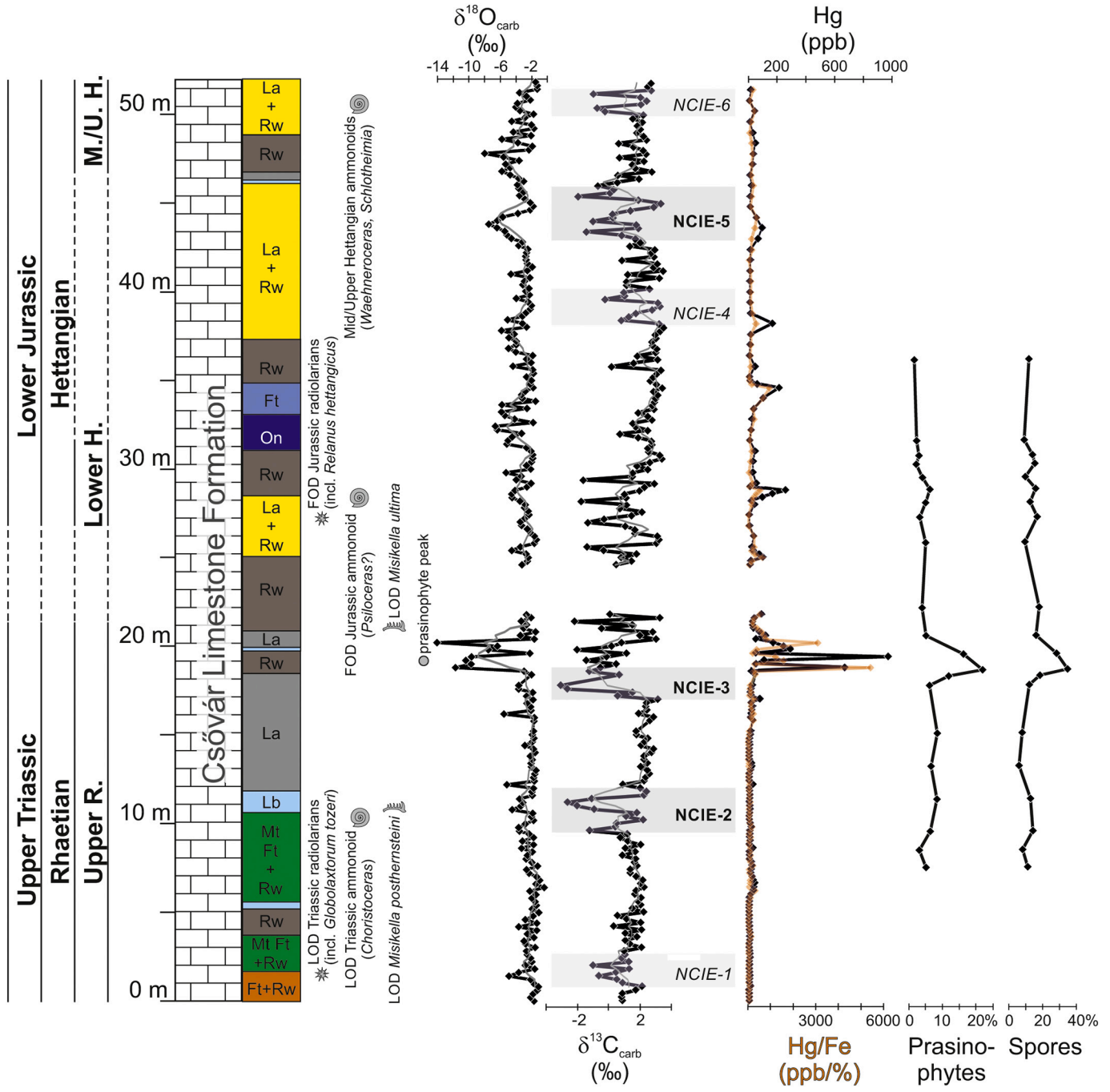

Fig. 4. New $\delta^{18}O$, $\delta^{13}C_{carb}$, Hg and Hg/Fe concentration data from the Csővár, Vár-hegy section. The light-grey curves are the 5-point running averages for $\delta^{18}O$, $\delta^{13}C_{carb}$ curves, respectively. Lithostratigraphic and microfacies log is modified from Haas and Tardy-Filácz (2004). Ft: fine-grained turbidite, Mt: medium-grained turbidite, Rw: radiolarian wackestone, La: calcisiltite-calcilutite laminate, Lb: lithoclastic-bioclastic grainstone/packstone, On: oncoid, grapestone grainstone/packstone/wackestone. Biostratigraphy is from Pálfy and Dosztály (2000), Pálfy et al. (2001), Götz et al. (2009) and this study. The palynological data is from Götz et al. (2009).

preserved, especially in the marly, laminated beds (Pálfy and Dosztály, 2000). The lowermost 10 m of the section yielded Rhaetian ammonoids (*Choristoceras* spp., *Cladiscites* sp.). At 19 m the first Jurassic phylloceratid was found *ex situ* and identified as *Nevadaphyllites psilomorphum* (Pálfy et al., 2001). The lowermost Jurassic ammonoid that occurs *in situ* was discovered at 29.5 m (*Psiloceras* sp.), representing the lower Hettangian. From the top of the section (Pálfy and Dosztály, 2000) reported a finding of *Waehneroceras* (~54 m), which suggests a middle Hettangian age. However, new finds of *Schlotheimia* sp. accompanied by Juraphyllitidae gen. et sp. indet., discovered near the same level during this study (~52 m), indicate the base of the upper Hettangian Marmorea Zone (see Appendix A.3.).

3.2. Radiolarian biostratigraphy

Although previous studies established a broad radiolarian biostratigraphy of Vár-hegy (Kozur and Mostler, 1990; Kozur, 1993), Pálfy et al. (2007) were the first to constrain the TJB in the section. Radiolarians at ~1.5 m represent the *Globolaxtorum tozeri* zone of late Rhaetian age, whereas radiolarians from ~26.5 m are assigned to the

Relanus hettangicus zone of early Hettangian age (Kozur and Mostler, 1990).

3.3. Conodont biostratigraphy

The bottom of the section (Bed 1) yielded a conodont fauna thought to belong to the *Misikella posthernsteini* zone (Kozur and Mock, 1991; Pálfy et al., 2001, 2007). Conodonts from 1.5–10.5 m were assigned to the *Misikella ultima* zone. However, recently Karádi (2018) proved the first occurrence of *M. ultima* significantly lower in the Csővár Fm., hence suggesting that the lower part of the Vár-hegy section lies entirely within the upper part of the revised *M. ultima* zone (Karádi et al., 2019). At 31.7 m *Neohindeodella detrei* was found, which is considered the sole survivor of the end-Triassic extinction in the conodont fauna (Kozur, 1993; Pálfy et al., 2001, 2007), although its occurrence could not be reproduced during this study. Taken together, biostratigraphy of primary age-diagnostic fossils (ammonoids, conodonts, radiolarians) establish an uppermost Rhaetian to middle-upper Hettangian chronostratigraphic range of the Vár-hegy section.

3.4. Foraminiferan biostratigraphy

The lowest part of the section (0–12.5 m) has an abundant and diverse Rhaetian foraminifera fauna (Pálfy et al., 2007). Above 12.8 m only impoverished assemblages are found. Platform-derived taxa are generally scarce in the section, however above 34.7 m, only neritic–bathyal fauna is described. The first Jurassic foraminiferan species (*Involutina liassica*) was identified from Bed 119, at 52 m.

3.5. Palynology

Palynological and palynofacies analyses were carried out in the interval of 7–37 m in the section (Götz et al., 2009). The lower part of the section yielded a late Rhaetian palynomorph assemblage. At ~19 m, there is a sudden increase of prasinophytes (*Tasmanites*), and trilete spores (*Concavisporites spp.*, *Deltoidospora spp.*) reach their peak abundance. The Hettangian assemblage (26–37 m) suggests a distal basinal setting, based on the presence of degraded organic matter, small equidimensional phytoclasts and foraminiferal test linings. The palynofacies patterns imply a continuously increasing continental influx and a change in the terrestrial vegetation in the hinterland.

3.6. Chemostratigraphy

The Vár-hegy section at Csővár was one of the first TJB sections where a NCIE was reported (Pálfy et al., 2001). With values ranging from -3.9‰ to 3.2‰ in the previously published $\delta^{13}C_{carb}$ data, the two main features of the curve are a smaller negative peak in the Rhaetian and a more significant one at the top of the Triassic strata (Pálfy et al., 2001, 2007). The major negative anomaly was further shown by a high-resolution resampling of the boundary interval, which revealed several smaller, temporally closely-spaced negative shifts within the excursion (Pálfy et al., 2007). Values fluctuate from -30.2‰ to -27.5‰ in the $\delta^{13}C_{org}$ curve and a prominent negative excursion is observed nearly coincident with the larger negative $\delta^{13}C_{carb}$ anomaly (Pálfy et al., 2001, 2007). As the NCIE around 19 m has been detected in both the $\delta^{13}C_{carb}$ and $\delta^{13}C_{org}$ data, it was thought to represent a primary signal. Previously measured $\delta^{18}O$ values fluctuate between -3.2‰ and -0.2‰, however some extreme (down to -10.3‰) negative values were measured as well (Pálfy et al., 2001, 2007).

3.7. Organic matter characterization

The total organic carbon content (TOC) was found to remain below 0.1% in the section (Pálfy et al., 2001). Based on the hydrogen index (HI), the organic matter is of marine origin. The variation in the amount of insoluble residue has a similar pattern to the TOC fluctuation, both of which, along with HI have a distinct decline at the top of the Triassic. HI* and the $\delta^{13}C_{org}$ show a reverse correlation in turbidites but not in the basinal facies. This was attributed to the fact that the organic matter in turbidites consists largely of isotopically heavy terrestrial particles, which have a low H-content (Pálfy et al., 2007).

3.8. Magnetostratigraphy

Magnetostratigraphy of the section was also investigated, with the aim of finding the short reversed polarity zone in the latest Rhaetian (Pálfy et al., 2007). This study established that the dominant carrier of remanent magnetism in the section is magnetite, revealing normal polarity throughout most of the section. However, in the Triassic–Jurassic transition interval, goethite, which occurs as alteration product after pyrite, generated a false, post-depositionally acquired signal of reversed polarity.

4. Material and methods

4.1. Sampling in the Csővár section

A total of 243 rock samples with 20 cm spacing were collected from the Vár-hegy section at Csővár (see Appendix Table A.1.). The sampled profile is identical to that reported in Pálfy et al. (2001, 2007). Only fresh, unweathered hand specimens were picked with an average size of 3x6x1 cm. A 2.7 m long interval between 21.8–24.6 m, above the previously identified *initial* CIE, was excluded from sampling as it consists of slumps. All new isotopic and Hg analyses were done on the same set of samples, albeit with a different measurement resolution.

In order to assess the reliability of the carbon isotope record in the section, two 20 cm thick slabs from individual beds of slightly different lithology were collected. One of them represents a hard, homogeneous limestone layer (Bed 19 at 7 m) and another one with softer, more marly lithology (Bed 18 at 6.6 m). These slabs were sampled at a high resolution (~1 cm) by micro-drilling (see Appendix A.1., Figures A.1., A.2, Tables A.4. and A.5.).

4.2. Stable carbon and oxygen isotope analysis

The entire suite of 243 samples collected from the section, with a 20 cm resolution, was processed for $\delta^{13}C_{carb}$ analysis. Each sample was drilled with a Proxxon Micromot 50/E drill (5000/min power) to obtain powder. Calcite veins were avoided. Stable carbon and oxygen isotope compositions were determined by reacting carbonate powder samples (150–200 μg) with orthophosphoric acid at 72 °C (Spötl and Vennemann, 2003) and analyzing the evolved CO_2 by an automated GASBENCH II sample preparation device attached to a Thermo Finnigan Delta Plus XP isotope ratio mass spectrometer (IRMS) at the Institute for Geological and Geochemical Research (IGGR, Budapest, Hungary). Three laboratory standards calibrated with the NBS-18, NBS-19 and LSVEC standards (provided by the International Atomic Energy Agency) were used for inter- and cross-laboratory standardization. A Harding Iceland Spar (Landis, 1983) sample was measured as unknown in the course of the study, and yielded $\delta^{13}C$ and $\delta^{18}O$ values of –4.82 ± 0.07 ‰ and –18.53 ± 0.07 ‰ (n = 20), respectively. These values are close to the published values of -4.80 and -18.56‰, respectively (Landis, 1983). On the basis of these results, the accuracy and reproducibility of $\delta^{13}C$ and $\delta^{18}O$ values are better than ± 0.1‰.

4.3. TOC analysis

A suite of 123 samples were selected for total organic carbon (TOC) analysis, at 20 cm resolution from 0 to 22 m, and at 60 cm resolution from 22 to 28 in the studied succession. The powdered samples were measured at the Earth Surface Research Laboratory (ESRL) at the

Department of Geology at Trinity College Dublin, The University of Dublin. For total inorganic carbon (TIC) measurement an average of 50 mg of powder was weighed, whereas for total carbon (TC) measurement an average of 80 mg was weighed. Both TIC and TC were measured on an *analytikjena®*, multi EA 4000 elemental analyser. To the TIC samples 30-40% H_3PO_4 acid was added automatically and the resulting CO_2 was introduced into the EA device. For TC analyses, carbon in a sample was oxidized to CO_2 (in an oxygen flow) at high temperature (~1200 °C). In both cases the results were expressed as % values. To obtain TOC values, TIC values were subtracted from the TC values. The detection limit was ~0.03%. Six samples were measured in duplicate or triplicate for total carbon (TC) and total inorganic carbon (TIC) concentrations (and thus calculated TOC concentrations), which covered an average TOC-concentration range of ~0.01 to ~0.9%. The standard deviation on the duplicate or triplicate measurements lies between 0.02 and 1.3%.

4.4. Mercury analysis

A suite of 163 rock samples were selected for mercury analysis, at 20 cm resolution from 0 to 26 m, and at 60 cm resolution from 26 to 52 m in the studied succession. The selected samples were powdered with an agate mortar and pestle. The mercury analysis was performed in the Earth Surface Research Laboratory (ESRL) at the Department of Geology at Trinity College Dublin, The University of Dublin, on a LECO AMA-254 mercury analyser, using the methodology described by Hall and Pelchat (1997). An average of 115 mg per samples was weighed on a scale. During the initial test measurements, it became obvious that, due to extremely low Hg concentrations, the standard 'isolation-mode' is inadequate for these samples, as it would often yield negative ppm values. To avoid this problem, all samples were measured in 'blank-mode' (on the same machine), which provides an absolute quantity of analyzed Hg (in ng). The obtained absolute Hg-concentrations were

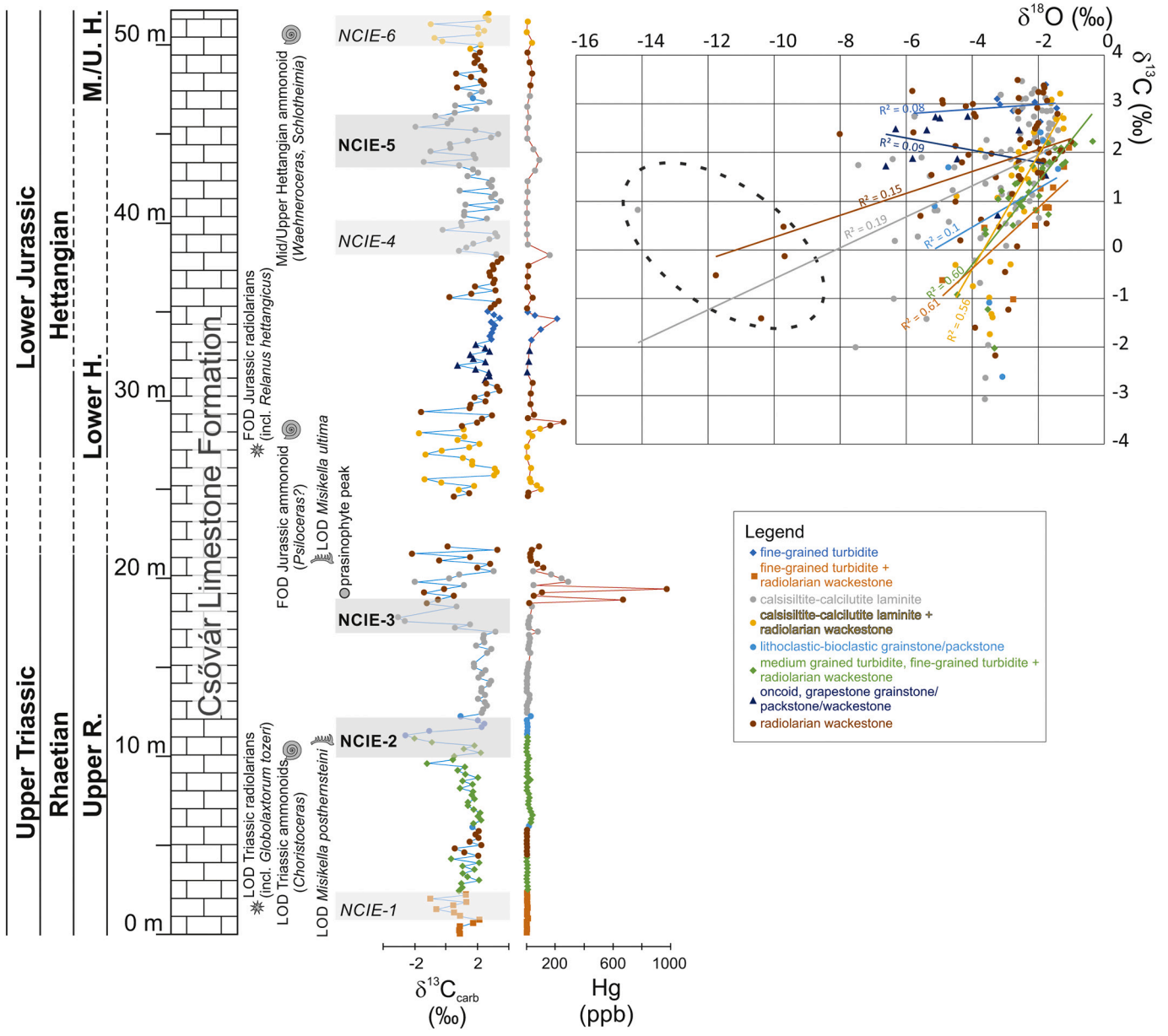

Fig. 5. New $\delta^{13}C_{carb}$ and Hg data with each microfacies represented by different colours, as well as a cross-plot diagram of the new $\delta^{13}C_{carb}$ and $\delta^{18}O$ values. The linear trendlines and the correlation coefficients (R^2) were calculated for each microfacies. The circle indicates a distinct group of samples with extremely low $\delta^{18}O$ values. Lithostratigraphic and microfacies log is modified from Haas and Tardy-Filácz (2004). Biostratigraphy is from Pálfy and Dosztály (2000), Pálfy et al. (2001), Götz et al. (2009) and this study.

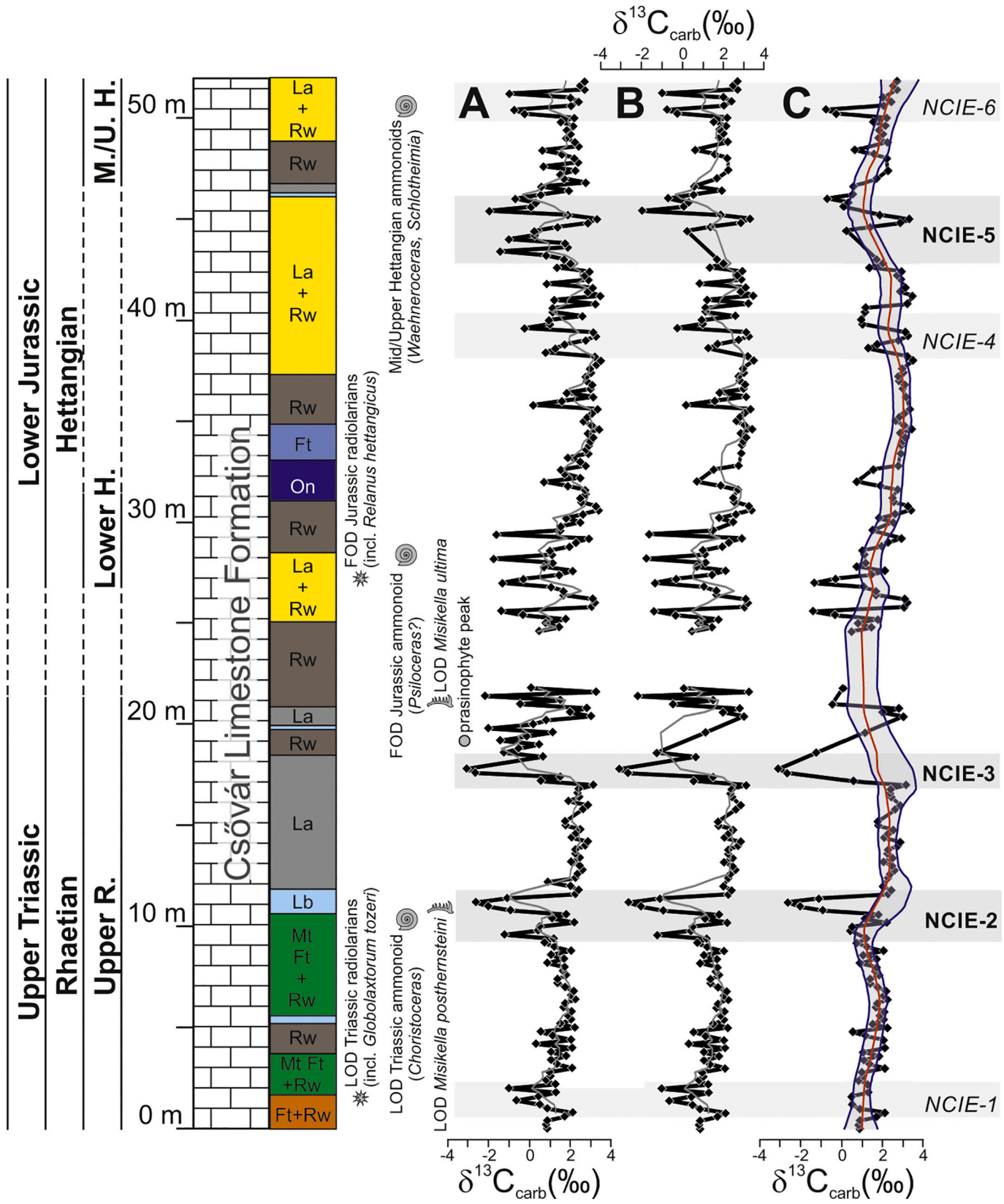

Fig. 6. $\delta^{13}C_{carb}$ curves of Csővár, Vár-hegy section. (A) The entire new $\delta^{13}C_{carb}$ dataset. The light-grey line is the 5-point running average. (B) Screened $\delta^{13}C_{carb}$ curve, after omission of samples with $\delta^{18}O$ values under -5‰. The light-grey line is the 5-point running average. (C) A further screened $\delta^{13}C_{carb}$ curve, after omission of single-point spikes, and LOESS smoothed curve (f = 0.1) of this screened $\delta^{13}C_{carb}$ dataset. Lithostratigraphic and microfacies log is modified from Haas and Tardy-Filácz (2004). Ft: fine-grained turbidite, Mt: medium-grained turbidite, Rw: radiolarian wackestone, La: calcisiltite-calcilutite laminate, Lb: lithoclastic-bioclastic grainstone/packstone, On: oncoid, grapestone grainstone/packstone/wackestone. Biostratigraphy is from Pálfy and Dosztály (2000), Pálfy et al. (2001), Götz et al. (2009) and this study.

subsequently calculated offline to obtain a concentration value. In cases of high (> 5 ng) values, blanks were analysed and/or test measurements were done between successive samples to exclude the possibility of internal Hg contamination. Every fifth sample was measured twice. The standard deviation on duplicate measurements is 1.18 ppb, and the difference between duplicates is (on average) ~3.95% the average of duplicates (see Appendix Table A.2.).

Some samples were also analysed in 'isolation-mode' (providing a direct 'online' approximation of sedimentary Hg concentrations). Obtained sedimentary Hg concentrations analysed and calculated offline (blank-mode) and online (isolation mode) agree well in the concentration range of 45–1000 ppb (with a linear correlation and R^2 = 0.99, n = 15 (excluding 3 outliers). The correlation between the two different measurement modes decreases exponentially when concentrations are towards the ppb range. Only blank-mode values are reported and discussed in the figures and text of the main manuscript, but all data and further discussion is provided in Appendix A.6., Table A.3.).

5. Results

5.1. $\delta^{13}C_{carb}$ and $\delta^{18}O$

Throughout the section, $\delta^{13}C_{carb}$ values vary considerably between -3.07‰ and 3.49‰, with an average of 1.51‰ (Fig. 4) (see Appendix Table A.1.). Although a slightly increasing trend is apparent overall, the most prominent feature is the presence of a series of negative carbon isotope excursions (NCIEs) of different amplitude and stratigraphic extent, labelled here successively from NCIE-1 to NCIE-6 (Fig. 6). The stratigraphically first NCIE, at the base of the section, has an amplitude of ~3‰ (NCIE-1 at 1.4–2 m). This is followed by another anomaly of ~-5‰ (NCIE-2 at 9–11.6 m). Above the last observed Triassic biostratigraphical marker, at 17 m, there is a sudden, significant drop in $\delta^{13}C_{carb}$ values of over 6‰ (NCIE-3 at 17–18.4 m). Following the TJB, in the upper part of the section, the $\delta^{13}C_{carb}$ values fluctuate noticeably, with three smaller negative excursions observed (NCIE-4 at 38–39.6 m, NCIE-5 at 45.4 m, and NCIE-6 at the top of the section). $\delta^{18}O$ values vary between -14.12‰ and -0.34‰ along the section, with greater magnitude in the upper half. The minimum value (-14.12‰) is observed at around 20 m, near NCIE-3.

5.2. TOC

Out of the total of 123 samples, only 39 measurements were above detection limit (0.03%) and TOC content remains below 2% throughout the section (see Appendix Table A.1.). The measured values vary between 0.03–1.84%, and only for 10 samples exceed 0.5%. There is no clear trend or pattern as the peak values are isolated at the base of the section, at 3.0 m and 15.2 m.

5.3. Sedimentary Hg concentrations

Mercury concentrations are overall very low in the lowest part of the section (from 0–5.8 m), with an average of 3.39 ppb (Fig. 4; see Appendix Table A.1.). In the interval of 5.8–8 m, Hg values rise to 40.8 ppb, but then gradually return to lower values of on average 2.13 ppb. Generally low (< 10 ppb) sedimentary Hg concentrations from 8 to 14.6 m are interrupted by four minor peaks of 27 ppb (at 8.6 m), 17 ppb (at 9.8 m), 29 ppb (at 12.2 m) and 20 ppb (at 13.2 m). At 14.8 m the sedimentary Hg values start to increase and reach 76 ppb at 17 m, followed by a decrease to 11 ppb at 17.4. Values vary greatly from 17.6–21.8 m, with peak concentrations of 668 ppb at 18.8 m and 972 ppb at 19.4 m. In the upper half of the section, sedimentary Hg concentrations are on average lower than in the interval from 18–22 m, but with several distinct peaks at 25 m (98 ppb), 28.8 m (256 ppb), 34.6 m (212 ppb), 38.2 m (164 ppb) and 43.6 m (91 ppb).

6. Discussion

6.1. Correlation of $\delta^{13}C_{carb}$ and $\delta^{18}O$ and the possible impact of diagenesis

The new Csővár $\delta^{13}C_{carb}$ and $\delta^{18}O$ records presented here show the same general trends observed in previous studies (Pálfy et al., 2001, 2007). The obtained data may reflect, to some extent, diagenetic alteration of the studied carbonates (Brand and Veizer, 1981; Veizer et al., 1999). A cross-plot between $\delta^{13}C$ and $\delta^{18}O$ values shows a distinct grouping of samples with significantly lower $\delta^{18}O$ values (Fig. 5). The majority of samples, however, show $\delta^{13}C$ and $\delta^{18}O$ values that are expected for diagenetically unaltered sediments, without a clear cross-correlation (with an average R^2 value of 0.3 for the entire data-set (excluding the outliers)), similar to observed by Pálfy et al. (2007).

Previous analyses identified and characterized several microfacies types in the section (Haas and Tardy-Filácz, 2004), and those results were used to examine if there is any correlation between depositional processes and the isotopic composition of the samples. Generally, $\delta^{18}O$ versus $\delta^{13}C$ cross-plots of the microfacies subsets reveal no facies-control on the chemical composition of the studied sediments. Only samples with oncoidal grapestone microfacies show a slight diagenetic trend, albeit with a very low R^2 of 0.09 (n = 11; Fig. 5). This is likely due a second phase of cementation, controlled by meteoric water, following the formation and deposition of the oncoids, which causes a shift towards more negative $\delta^{18}O$ values (Pederson et al., 2015).

6.2. Interpretation of the $\delta^{13}C_{carb}$ record

To assess and ensure that the obtained $\delta^{13}C_{carb}$ data (Fig. 6A)can be reliably interpreted to reflect changes in the $\delta^{13}C$ of DIC in the basin, across the studied stratigraphic interval, and as captured in the studied stratigraphic record, three approaches were employed. Firstly, $\delta^{13}C$ data from samples with low $\delta^{18}O$ values (below -5‰), commonly associated with diagenetic alteration (Brand and Veizer, 1981), were omitted (Fig. 6B). Secondly, single-point spikes in $\delta^{13}C_{carb}$ were omitted, where a single value differs more then ~2‰ from the average of the pre- and succeeding samples (Fig. 6C). This was justifiable because of the observations from the preliminary analyses of the two 20 cm thick slabs, which showed that even within a 20 cm rockslab individual spikes occur that most probably are not the result of change in the carbon cycle (see Appendix A.1., Figures A.1., A.2, Tables A.1., A.4. and A.5.). Thirdly, a LOESS smoothing (f = 0.1) was performed for the remaining dataset with the originally identified NCIEs (NCIE-1 to NCIE-6) also apparent in the LOESS smoothed curve (Fig. 6C). As NCIE-1–6 are all recognized on all the curves, they are interpreted as primary signals, thus a reflection of changes in the carbon cycle. Out of these six anomalies, NCIE-2, -3, and -5 are the most prominent excursions, with NCIE-3 being the most significant.

6.3. Carbon isotope excursions at Csővár and their correlation with other TJB sections

The $\delta^{13}C$ curve obtained at Csővár likely reflects changes in, or perturbations to, the global exogenic carbon cycle; this is tested by comparison of the Csővár $\delta^{13}C$ record with stratigraphically overlapping $\delta^{13}C$ records from other Triassic–Jurassic boundary sections where Hg data are also available (Fig. 7). The $\delta^{13}C_{org}$ record from the marine TJB section at St. Audrie's Bay, SW England, is marked by three NCIEs (Hesselbo et al., 2002; Ruhl and Kürschner, 2011). The lowermost is a ~2‰ negative excursion in the uppermost Rhaetian, referred to as the *precursor* CIE (Ruhl and Kürschner, 2011). The most significant anomaly in the section is a sharp ~4‰ NCIE, named as the *initial* CIE, at the same stratigraphic level as the end-Triassic mass extinction (ETE), based on sporomorphs and dinoflagellates (Hesselbo et al., 2002). The youngest NCIE was identified higher in the section, starting below the base of the *Psiloceras planorbis* Zone in that section, and

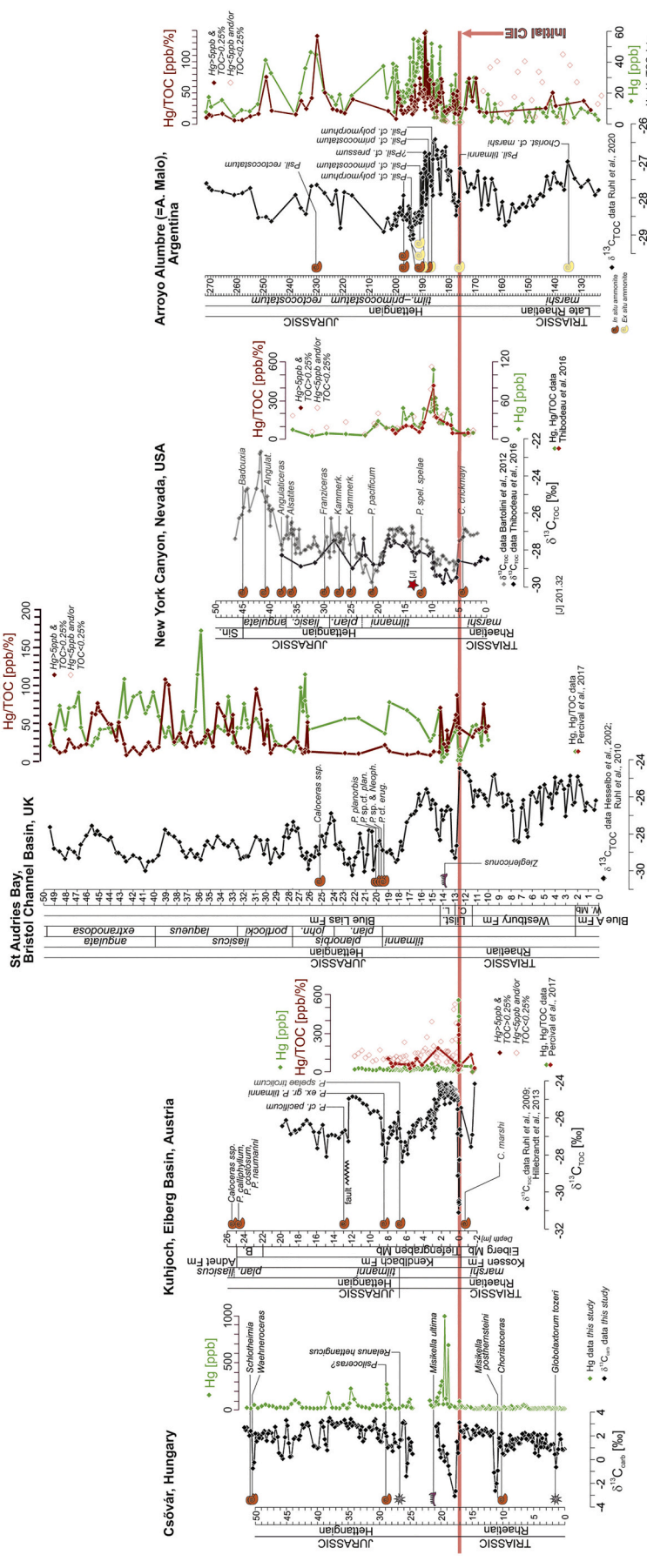

Fig. 7. The new $\delta^{13}C_{carb}$ and Hg concentration data from Csővár compared to other TJB sections' $\delta^{13}C_{org}$ and Hg/TOC data (*This study*; Hesselbo et al., 2002; Ruhl et al., 2009; Ruhl et al., 2010; Bartolini et al., 2012; Hillebrandt et al., 2013; Thibodeau et al., 2016; Percival et al., 2017; Ruhl et al., 2020). The Hg/TOC is screened by low TOC and/or Hg concentration. The positions of biostratigraphical markers are indicated next to each section. For Csővár, the biostratigraphy is from Pálfy and Dosztály (2000), Pálfy et al. (2001) and this study. For Kuhjoch, the biostratigraphy is from Hillebrandt et al. (2013). For St. Audries Bay, the biostratigraphy is from Swift (1995) and Weedon et al. (2019). For New York Canyon (Ferguson Hill), the biostratigraphy is from Guex et al. (2004), Lucas et al. (2007) and Bartolini et al. (2012). For Arroyo Alumbre, the biostratigraphy is from Riccardi (2019).

referred to as the *main* CIE (Hesselbo et al., 2002). It is less sharp and much longer-lived than the earlier CIEs, continuing well into the Sinemurian (Ruhl et al., 2010b; Hüsing et al., 2014; Hesselbo et al., 2020).

The Global Stratotype Section and Point (GSSP) for the base of the Hettangian Stage is defined in the Kuhjoch section in the Northern Calcareous Alps, Austria (Hillebrandt et al., 2013). There, and in the Eiberg section, the first anomaly in organic carbon isotopes occurs in the uppermost Rhaetian and is identified as the *precursor* CIE (Ruhl and Kürschner, 2011), although earlier, mid and upper Rhaetian negative CIEs have also been identified there (Mette et al., 2012; Korte et al., 2017; Mette et al., 2019; Rizzi et al., 2020). A sharp and high-amplitude (~5‰) NCIE was detected at the top of the Kössen Formation, identified as the *initial* CIE (Ruhl et al., 2009). Stratigraphically above the subsequent Schattwald beds and above the first occurrence of *Psiloceras spelae*, in the nearby Ochsentaljoch section, another NCIE of lower amplitude but longer duration develops that lasts up to the top of section and is identified as the *main* CIE (Ruhl et al., 2009; Korte et al., 2019).

The Triassic–Jurassic boundary in the terrestrial Astartekløft section, SE Greenland, is marked by a definite (~3.5‰) negative shift in the $\delta^{13}C_{wood}$ record across the TJB, defined by the transition from the *Lepidopteris* macrofloral zone to the *Thaumatopteris* zone (Hesselbo et al., 2002). As $\delta^{13}C_{wood}$ values remain low in the upper part of the section, this CIE was correlated with the onset of the *main* CIE at the base of the Hettangian, in agreement with palynostratigraphy (Mander et al., 2013). Although there is no unequivocal record of the earlier CIEs here, low data resolution and likely stratigraphic hiatuses in this fluvio-deltaic succession leave open the possibility of their presence. Importantly, fossil leaves collected from this section allowed for stomatal density analyses and reconstruction of atmospheric pCO_2 change at this time (McElwain et al., 1999)

The Triassic–Jurassic transition at New York Canyon, Nevada, is marked by a distinct NCIE, identified as the *initial* CIE, stratigraphically closely following the last occurrence of *Choristoceras crickmayi* (Guex et al., 2004; Ward et al., 2007; Bartolini et al., 2012; Thibodeau et al., 2016). The proposed record of the *main* CIE here (Bartolini et al., 2012; Thibodeau et al., 2016) is controversial for its brevity in comparison with other sections.

The carbon isotope record of the Triassic–Jurassic transition at the marine Arroyo Alumbre section (Arroyo Malo, Neuquén Basin, Argentina) is marked by a definite NCIE (~1.5‰ in amplitude within a dataset of ~2.5‰ total range), identified as the *initial* CIE. This is followed in the lowermost Jurassic by a greater and more prolonged negative shift which can be correlated with the *main* CIE (Ruhl et al., 2020).

At Csővár, NCIE-3 is the most significant anomaly of the section and is identified here with the *initial* CIE that can be best used for global correlation as it coincides with the ETE horizon (Hesselbo et al., 2002; Ruhl et al., 2009; Korte et al., 2019). Peak abundance of prasinophytes and spores occurs at the same stratigraphical level as NCIE-3, which indicates major and synchronous changes in marine and terrestrial ecosystems and permits stratigraphic correlation with sections with similar features (e.g. the Newark Basin (US; Olsen et al., 2002), St Audries Bay (UK; Deenen et al., 2010), the Germanic Basin (Germany and Denmark; van de Schootbrugge et al., 2009; Lindström et al., 2012), and the Sichuan Basin (China; Li et al., 2020), even when *C. thiergartii*, the terrestrial auxiliary marker for the base of the Jurassic, is not observed (Götz et al., 2009; Hillebrandt et al., 2013; Lindström et al., 2017). Based on its shape and position below the *initial* CIE, NCIE-2 in the Vár-hegy section and the correlative NCIE from the Pokol-völgy quarry (Korte and Kozur, 2011) may be tentatively identified as the *precursor* CIE (Ruhl and Kürschner, 2011). However, considering that the total thickness of the Rhaetian at Csővár exceeds 80 m (Karádi et al., 2019), this correlation is uncertain, as NCIE-2 at Csővár may be stratigraphically higher than the *precursor* CIE in other sections. The *main* CIE, as identified at St Audrie's Bay (Hesselbo et al., 2002), with a negative shift followed by a period that is characterized by rather large oscillations with Milankovitch frequencies, cannot be observed at Csővár with any certainty as opposed to other TJB sections. However, as there appears to be regional variability in significance and duration of the *main* CIE (Hesselbo et al., 2002; Guex et al., 2004; Ruhl et al., 2009; Ruhl et al., 2010a; Lindström et al., 2012; Hüsing et al., 2014; Thibodeau et al., 2016; Lindström et al., 2017; Percival et al., 2017; Xu et al., 2017; Hesselbo et al., 2020; Storm et al., 2020), there is a possibility that NCIE-5 is the *main* CIE at Csővár.

6.4. Mercury anomalies at Csővár and their correlation with other TJB sections

Generally low sedimentary Hg concentrations observed in the uppermost Triassic (the first 18 m) of the studied Csővár section are interpreted as showing a pre-volcanic background signal. Upsection, a major enrichment in sedimentary Hg coincides with the NCIE-3 and is followed by five smaller but distinct enrichments (Fig. 4). The increase in sedimentary Hg concentrations starts simultaneously with the onset of the *initial* CIE (or NCIE-3) and reaches a maximum value of > 970 ppb, 1 m above the onset. Four of the successive minor Hg peaks, all with values > 90 ppb, occur stratigraphically near smaller negative shifts in the $\delta^{13}C_{carb}$ data. Due to the overall very low TOC values in the section (see Appendix Table A.1.), the Hg/TOC normalization established and recommended in numerous similar studies cannot be applied at Csővár as it would lead to false Hg/TOC peaks due to the relatively large % analytical error on low TOC sample measurements (Sanei et al., 2012; Grasby et al., 2019 and references therein). Given the observed extreme variations in sedimentary Hg-concentrations, it appears that in the Csővár succession organic matter enrichment is not the controlling factor on sedimentary Hg values across the Triassic–Jurassic transition. As additional controlling factors, detrital input and sulphide segregation have also been proposed (Grasby et al., 2019; Shen et al., 2019b, 2020). We obtained new elemental geochemical data through XRF analysis (see Appendix A.5.). Neither the Al nor the S data allow their use for normalization due to their overall low concentration that often remains below detection limit and resulted in an incomplete dataset. However, Fe data is obtained for all samples, and since Fe-sulphides constitute the most common sulphide minerals, and Fe concentration may increase through detrital input, we employed Hg/Fe normalization (see Appendix Table A.1.). As the Hg concentration curve is parallel with the Hg/Fe curve (Fig. 4), it appears that neither sulphide precipitation, nor detrital input govern the change in the sedimentary Hg concentration. Furthermore, the studied succession is not marked by major lithological changes, nor do changes in sedimentary Hg concentrations correlate with variations in microfacies-type, suggesting that lithology is of no apparent control on the sedimentary Hg-signal (see Fig. 5).

Geographically near (e.g. at Kuhjoch, Eiberg Basin, Austria (Percival et al., 2017)) as well as far away (e.g. at Ferguson Hill/ NewYork Canyon, Nevada, USA (Thibodeau et al., 2016) or Arroyo Alumbre, Argentina (Ruhl et al., 2020)), sedimentary archives show a similar Hg signal across the Triassic–Jurassic transition compared to Csővár, with a major spike in sedimentary Hg during or stratigraphically close to the *initial* CIE and followed by subsequent, smaller peaks in sedimentary Hg abundance (Fig. 7).

Compared to other TJB sections, Csővár stands out for its significantly higher Hg concentration peak, with values of up to 972 ppb (where sedimentary Hg concentrations at Kuhjoch peak at 555 ppb and in the Rødby-1 core peak at 550 ppb (Percival et al., 2017; Lindström et al., 2019). Some TJB sections, however, show only very limited sedimentary Hg concentrations or signals that appear stratigraphically different to what is observed here. This has also been observed for other time-intervals marked by large igneous province volcanism, such as during the Toarcian Oceanic Anoxic Event, the Cretaceous-Paleogene

event and at the Paleocene–Eocene Thermal Maximum (Percival et al., 2018; Jones et al., 2019) and it may largely be due to local and regional processes impacting on the shuttling of Hg from the atmosphere/ocean into the sedimentary depositional environment.

Despite regional differences in Hg deposition, the stratigraphical onset of enriched sedimentary Hg concentrations in geographically widespread locations appears to coincide with elevated atmospheric pCO_2 and a major carbon cycle perturbation, as represented by the *initial* CIE, and the onset of extrusive volcanism associated with CAMP emplacement (Percival et al., 2017).

The combined effect of the elevated temperature and the release of CO_2 and other gases and toxic metals likely contributed to the synchronous mass extinction (McElwain and Chaloner, 1995; McElwain et al., 1999; Ward et al., 2001; Pálfy et al., 2002; Steinthorsdottir et al., 2011; Bond and Grasby, 2017; Lindström et al., 2019; Li et al., 2020).

6.5. Causes of NCIEs and Hg anomalies

The generally low Hg values in the lower part of the section (0–17 m) is interpreted as representing a pre-CAMP background signal, which corresponds well with data from sedimentary records that formed during the emplacement of other LIPs (e.g. Grasby et al., 2015, 2019; Wang et al., 2019). On the $\delta^{13}C$ curve of this interval, NCIE-2 may be identified as the *precursor* CIE. This stratigraphic interval is characterized by the two negative CIEs of which NCIE-2 is the more prominent one (Fig. 4). Previous studies recorded negative CIEs, preceding the end-Triassic mass extinction and commonly termed *precursor* CIEs, and suggested these to reflect global carbon-cycle perturbations preceding the onset of the main CAMP emplacement (Ruhl and Kürschner, 2011; Mette et al., 2012, 2019; Blumenberg et al., 2016; Korte et al., 2017; Fujisaki et al., 2018). Although the geological significance of the *precursor* CIE is debated, the most commonly proposed hypothesis posits that the NCIE is the result of the release of isotopically light CO_2 from contact metamorphism of organic-rich sediments during the intrusive phase of the CAMP activity (Davies et al., 2017; Heimdal et al., 2018). Sedimentary Hg concentrations are low throughout the lower part of the succession, with only a minor increase of up to 70 ppb at ~6m (Fig. 7), which stratigraphically predates NCIE-2 (the *precursor* CIE) by ~4 m (Figs. 4 and 7). This data suggests that early CAMP intrusives, which are suggested to have been responsible for carbon release and associated carbon-cycle perturbations predating the main phase of CAMP basalt emplacement, may have been accompanied by significant Hg release into the global ocean-atmosphere system, although the ratio between carbon and Hg degassing from sill intruded subsurface organic-rich shales may have varied over time (Heimdal et al., 2018, 2019; Ruhl et al., 2020).

In the biostratigraphically identified TJB transition interval, the most significant carbon isotope anomaly, NCIE-3, likely represents the *initial* CIE associated with the end-Triassic mass extinction. This major negative CIE is suggested to have resulted from CAMP basalt degassing, and possibly accompanied by ocean-floor methane hydrate dissociation (Ruhl et al., 2011; Capriolo et al., 2020), suggesting synchrony of paroxysmal volcanism and rapid global warming. The NCIE-3 in the Csővár record, identified as the *initial* CIE, is parallel with a major increase in sedimentary Hg concentrations, of up to 1000 ppb (Fig. 7). The simultaneous occurrence of the carbon isotope and Hg-anomaly is broadly in agreement with other TJB sections globally (Thibodeau et al., 2016; Percival et al., 2017; Lindström et al., 2019; Ruhl et al., 2020). The Hg-record from Csővár supports the scenario that the onset of a more explosive phase of CAMP volcanism may have injected Hg into the stratosphere, thereby allowing its global distribution (Thibodeau et al., 2016; Percival et al., 2017; Lindström et al., 2019; Ruhl et al., 2020).

Following the initial peak in Hg concentrations, the sedimentary Hg levels remained high compared to pre-volcanic background, with significant subsequent peaks in sedimentary Hg concentrations occurring throughout the Hettangian part of the succession. These subsequent Hg peaks may suggest episodic release of Hg, and CO_2, during later phases of CAMP volcanism (Percival et al., 2017; Lindström et al., 2019).

6.6. Possible causes and significance of high Hg concentration at Csővár

Low TOC values throughout the carbonate succession at Csővár suggest that changes in TOC cannot be a significant factor in the major fluctuations in Hg concentrations throughout the section. Furthermore, a global comparison of ranges in maximum sedimentary Hg concentrations and corresponding TOC values across the end-Triassic mass extinction and Triassic–Jurassic transition does not reveal any meaningful correlation between maximum TOC and sedimentary Hg concentrations (Fig. 8). The Hg-record at Csővár also appears unrelated to minor lithological changes, as reflected by variations in microfacies-type (see Fig. 5).

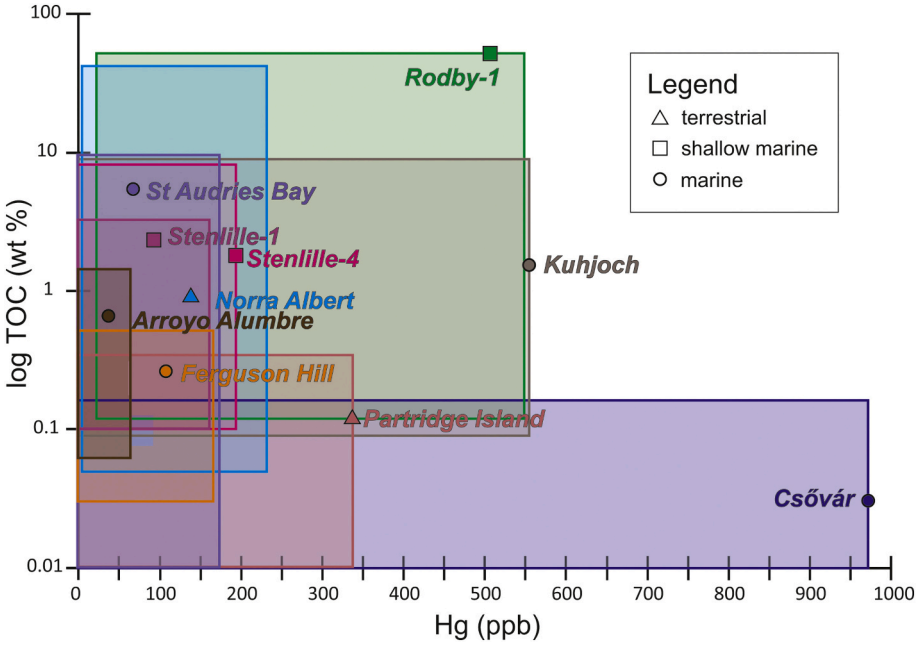

Fig. 8. The range of TOC and sedimentary Hg concentrations in different Triassic-Jurassic boundary successions; shown are the maximum Hg values coinciding with, or stratigraphically close to the *initial* CIE. Data from Pálfy et al. (2001), Thibodeau et al. (2016), Percival et al. (2017), Lindström et al. (2019), Ruhl et al. (2020) and this study.

The peak in sedimentary Hg coincident with the *initial* CIE (NCIE-3) at Csővár, exceeds all previously reported values for this stratigraphic interval in other TJB sections, and it appears unusually high, even though not entirely unprecedented, compared to sedimentary records of other global change events (Percival et al., 2018; Grasby et al., 2019). One possible explanation for the high peak in sedimentary Hg concentrations at Csővár lies in the pulsatory nature of CAMP volcanism (Marzoli et al., 2004, 2019; Deenen et al., 2010; Hachimi et al., 2011; Blackburn et al., 2013; El Ghilani et al., 2017; Percival et al., 2017, 2018; Panfili et al., 2019; Capriolo et al., 2020) and the short residence time (0.5–1 yr) of Hg in the atmosphere (Pyle and Mather, 2003; Selin, 2009; Wang et al., 2019). With this, the detection of sedimentary Hg-enrichment may be a case of 'hit or miss', depending largely on whether sediment was deposited, and preserved, locally during temporally elevated volcanic activity and associated atmospheric Hg-fluxes. The significantly larger Hg peaks at Csővár (reaching 972.14 ppb at 19.4 m) may therefore simply represent the serendipitous discovery of sedimentary layers that formed during individual CAMP volcanic pulses, aided by the presumably relatively complete sedimentary record, marked by relatively high sedimentation rates, at Csővár. Alternatively, high sedimentary Hg concentrations may be explained by the presence of cryptotephra, i.e. volcanogenic material, possibly enriched in Hg, within the section. Electron probe microanalysis (EPMA) on a sample with the second highest Hg value at 18.8 m revealed a porous, volcanoclastic-like microlayer of silicified Fe-oxides with apatite and barite plates without any orientation (see Appendix A.4.). The barite plates are partly resorbed, with pore spaces also filled with barite, suggesting formation shortly after deposition. The barite contains a noticeable amount of Sr, whereas the apatite is rich in Sr and REE. The EPMA analysis of a sample from 19.4 m identified altered Fe-oxides with apatite and Mg-rich biotite (phlogopite). The alteration of biotite is further supported by the elevated level of kaolinite found in these samples by X-ray diffractometry. These minerals are associated with dispersed Ba-Sr-REE-rich volcanic material that is typical of alkaline volcanic activity. Occurrence of such minerals is in accordance with observations of Bensalah et al. (2011) who associate the early phase of CAMP with alkaline volcanism. The observed possible cryptotephra were altered by interaction with diagenetic fluids as suggested by the exceptionally low $\delta^{18}O$ values, this layer may therefore have been further enriched in Hg by partial mobilization and redeposition from adjacent beds. However, the beds in question are texturally homogeneous distal calcareous turbidites and micro-fissures are rare. Therefore, the concept of fluid flow restricted to one particular bed may not be supported by sedimentological evidence (Haas and Tardy-Filácz, 2004). Additionally, Cretaceous bentonites that formed shortly before Oceanic Anoxic Event 2 (OAE2) in the Mevarick Basin of central Texeas (USA) have been proven to have low Hg concentrations (Scaife et al., 2017); consequently it may be unlikely that the presence of cryptotephra caused the high Hg concentration at Csővár.

Another possible explanation for the elevated sedimentary Hg level is the change of Hg-bearing mineral phases recorded in the TJB interval. It is possible that the Hg-bearing phase differs in geographically close locations (Shen et al., 2020). Previous magnetostratigraphic studies in the section revealed that the dominant magnetic mineral is magnetite throughout the section, except for the interval of 15–21 m, around the Triassic–Jurassic boundary. Here, a significant amount of goethite is present, which has been identified as alteration product after pyrite (Pálfy et al., 2007). Possibly, magnetite is the dominant Hg-carrying phase in the lower and upper part of the section (Dunham et al., 2003; Melamed and da Luz, 2006; Girginova et al., 2010; Ahmaruzzaman and Gupta, 2012; Yang et al., 2014, 2017). However, in the interval of 15–21 m (including the end-Triassic mass extinction interval), the observed altered pyrite in the form of goethite may have carried additional Hg (Benoit et al., 1999; Ravichandran, 2004; Pálfy et al., 2007). Microprobe analysis showed the presence of Zn-Hg sulphides, with a minor amount of Cd (see Appendix A.4.). After organic matter, sulphides are the second most significant carriers of Hg into sediments (Benoit et al., 1999; Ravichandran, 2004). Methylating bacteria, present in sulphide-rich sediment, capture Hg^0 from the porewater, which is evident by the correlation between the HgS^0 and MeHg concentrations in sediments (Benoit et al., 1999). The significance of pyrite in the Hg system is also supported by the observation of extremely high Hg concentrations (265–1547 ppb) detected in pyrite beds and pyrite-rich black shales (Shen et al., 2019a). A Hg-pyrite correlation has commonly been associated with anoxia, which did not occur at Csővár. However, under oxic/suboxic conditions Hg-release is possible from decomposed organic matter and it is taken up by sulphide phases (Shen et al., 2020). Therefore, the presence of the Hg-bearing magnetite possibly combined with sulphide-captured Hg may be considered as an explanation for the extremely high Hg concentration at Csővár. However, the lack of Fe-peaks at the Triassic–Jurassic transition at Csővár suggests no major changes in Fe-bearing minerals, thus also questioning whether sedimentary pyrite, or any sulphide, concentrations thoroughly explain the observed Hg-record.

7. Conclusions

New high-resolution $\delta^{13}C_{carb}$ data from the TJB section at Csővár builds on previously published data, showing six successive NCIEs of up to ~6‰ at the end-Triassic mass extinction interval. The uppermost Triassic NCIE-3, associated with the end-Triassic mass extinction, represents the most prominent and well-defined minimum in the section and provides a robust correlation with the *initial* CIE in other sections globally. The existence of a prolonged *main* NCIE, observed elsewhere, is not obvious in the Csővár section. The largest ~6‰ NCIE, associated with the end-Triassic mass extinction in the Csővár section likely represents a significant perturbation of the end-Triassic carbon cycle, resulting from CAMP volcanic degassing, possibly combined with, episodically released ^{12}C-enriched methane derived from gas hydrate dissociation and/or contact metamorphism.

Mercury analyses at Csővár shows that this proxy can reliably be used to study global Hg-fluxes and the evolution of the global Hg-cycle in homogeneous, organic-lean limestone successions. Here, TOC values are commonly too low to use for Hg normalization. The consistently low organic content excludes the possibility that changes in organic matter sequestration significantly controlled the observed stratigraphic changes in sedimentary Hg concentrations.

The Hg-record from Csővár presented here, spanning the upper Rhaetian to mid-upper Hettangian, shows relatively low pre-volcanic background values in the lower part of the succession. This is followed by a significant rise in sedimentary Hg near the *initial* CIE, similarly to other TJB sections. Sedimentary Hg values do not return to the background but remain elevated with occasional spikes, throughout most of the Hettangian in the studied succession.

The major Hg anomaly at the end-Triassic negative CIE is interpreted as the onset of the extrusive phase of CAMP activity, immediately following intrusive magmatic activity. Mercury levels are already enriched, albeit generally low, before the end-Triassic mass extinction interval, suggesting that early phases of intrusive magmatic activity associated with CAMP may have had some impact on Hg-fluxes into the atmosphere. Subsequent Hg spikes, following the end-Triassic mass extinction interval are smaller in magnitude but support a pulsatory nature of CAMP volcanism, possibly leading to prolonged stressed environments following the extinction event.

Significantly elevated sedimentary Hg concentrations at the end-Triassic mass extinction interval at Csővár are higher than at any other TJB succession, but comparable in magnitude to Hg anomalies at other global change events. The elevated Hg level may be because (1) the sampled succession was characterized by sedimentation and sediment preservation synchronous with a major eruption, thus immediately capturing the elevated Hg-fluxes into the atmosphere, (2) the preservation of cryptotephra, observed through electron microprobe

analyses, and represented by the presence of a thin, porous volcanoclastic-like microlayers, possibly enriched in Hg (although this is in disagreement with observations of Scaife et al., 2017 showing no Hg-enrichments in Cretaceous bentonites), (3) the dominant Hg-carrier phase in the basin and sedimentary pore-space changed through time, as reflected by a change from predominantly magnetite as Hg-bearing mineral in the lower and upper part of the succession, which is supplemented by pyrite (or goethite) as additional Hg-carrier at the end-Triassic mass extinction interval. This explanation is, however, complicated by the overall low and consistent Fe concentration record, suggesting limited to no major changes in iron-bearing mineral concentrations throughout the studied succession.

The new geochemical data from Csővár are in accordance with the emerging global scenario of the CAMP-related environmental crisis at the Triassic–Jurassic transition. The coincidence of the *initial* CIE, which correlates with the ETE horizon, and the major Hg anomaly provides new evidence to strengthen the cause-and-effect relationship between CAMP volcanism and the end-Triassic extinction.

Supplementary data to this article can be found online at https://doi.org/10.1016/j.gloplacha.2020.103291.

Declaration of Competing Interest

The authors declare that they have no known competing financial interests or personal relationships that could have appeared to influence the work reported in this paper.

Acknowledgements

We are grateful to Laura Bódi, Viktor Karádi, and Attila Lavaj for their help in field sampling, and Dóra Kesjár, Attila Horváth, Alexandra Müller, Bence Reitmeyer and László Szikszay for assistance in sample preparation and analytical work. Discussions with János Haas and Norbert Zajzon were insightful. We thank János Haas and Lawrence Percival for constructive comments on the first author's MSc thesis that formed the basis for this manuscript. Detailed and helpful comments by two anonymous journal reviewers led to a significantly improved manuscript. Travel funds from the Papp Simon Foundation are acknowledged. The research was supported by the European Union and the State of Hungary, co-financed by the European Regional Development Fund in the project of GINOP-2.3.2-15-2016-00009 'ICER'. Additional funding was received from the National Research, Development and Innovation Office (Grant No. NN 128702). Micha Ruhl and the geochemical analyses at Trinity College Dublin were supported by the Irish Centre for Research in Applied Geosciences (iCRAG). This is MTA-MTM-ELTE Paleo Contribution No. 325.

References

Ahmaruzzaman, M., Gupta, V.K., 2012. Application of coal fly ash in air quality management. Ind. Eng. Chem. Res. 51 (47), 15299–15314. https://doi.org/10.1021/ie301336m.

Bartolini, A., Guex, J., Spangenberg, J.E., Schoene, B., Taylor, D.G., Schaltegger, U., Atudorei, V., 2012. Disentangling the Hettangian carbon isotope record: implications for the aftermath of the end-Triassic mass extinction. Geochem. Geophys. Geosyst. 13 (1). https://doi.org/10.1029/2011gc003807.

Beerling, D.J., Berner, R.A., 2002. Biogeochemical constraints on the Triassic-Jurassic boundary carbon cycle event. Glob. Biogeochem. Cycles 16 (3). https://doi.org/10.1029/2001gb001637. 10-1-10-13.

Benkő, K., Fodor, L., 2002. Csővár környékének szerkezetföldtana (Structural geology near Csővár, Hungary). Földtani Közlöny 132 (2), 223–246.

Benoit, J.M., Gilmour, C.C., Mason, R.P., Heyes, A., 1999. Sulfide controls on mercury speciation and bioavailability to methylating bacteria in sediment pore waters. Environ. Sci. Technol. 33 (6), 951–957. https://doi.org/10.1021/es9808200.

Bensalah, M.K., Youbi, N., Mahmoudi, A., Bertrand, H., Mata, J., El Achimi, H.E., Madeira, J., Martins, L., Marzoli, A., Bellon, H., Medina, F., Karroum, M., Abbou, M.B., 2011. The Central Atlantic Magmatic Province (CAMP) volcanic sequences of Berrechid and Doukkala basins (Western Meseta, Morocco): volcanology and geochemistry. Comunicacoes Geologicas 98 (1), 15–27.

Blackburn, T.J., Olsen, P.E., Bowring, S.A., McLean, N.M., Kent, D.V., Puffer, J., McHone, G., Rasbury, E.T., Et-Touhami, M., 2013. Zircon U-Pb geochronology links the end-triassic extinction with the Central Atlantic Magmatic Province. Science 340 (6135), 941–945. https://doi.org/10.1126/science.1234204.

Blumenberg, M., Heunisch, C., Lückge, A., Scheeder, G., Wiese, F., 2016. Photic zone euxinia in the central Rhaetian Sea prior the Triassic-Jurassic boundary. Palaeogeogr. Palaeoclimatol. Palaeoecol. 461, 55–64. https://doi.org/10.1016/j.palaeo.2016.08.007.

Bond, D.P.G., Grasby, S.E., 2017. On the causes of mass extinctions. Palaeogeogr. Palaeoclimatol. Palaeoecol. 478, 3–29. https://doi.org/10.1016/j.palaeo.2016.11.005.

Bond, D.P.G., Wignall, P.B., Keller, G., Kerr, A.C., 2014. Large igneous provinces and mass extinctions: an update, volcanism, impacts, and mass extinctions: causes and effects. Geol. Soc. Am. https://doi.org/10.1130/2014.2505(02.

Bowman, K.L., Hammerschmidt, C.R., Lamborg, C.H., Swarr, G., 2015. Mercury in the North Atlantic Ocean: the U.S. GEOTRACES zonal and meridional sections. Deep-Sea Res. II Top. Stud. Oceanogr. 116, 251–261. https://doi.org/10.1016/j.dsr2.2014.07.004.

Brand, U., Veizer, J., 1981. Chemical diagenesis of a multicomponent carbonate system; 2, Stable isotopes. J. Sediment. Res. 51 (3), 987–997. https://doi.org/10.1306/212f7df6-2b24-11d7-8648000102c1865d.

Capriolo, M., Marzoli, A., Aradi, L.E., Callegaro, S., Dal Corso, J., Newton, R.J., Mills, B.J.W., Wignall, P.B., Bartoli, O., Baker, D.R., Youbi, N., Remusat, L., Spiess, R., Szabó, C., 2020. Deep CO_2 in the end-Triassic Central Atlantic magmatic province. Nat. Commun. 11 (1), 1670. https://doi.org/10.1038/s41467-020-15325-6.

Courtillot, V.E., Renne, P.R., 2003. On the ages of flood basalt events. Compt. Rendus Geosci. 335 (1), 113–140. https://doi.org/10.1016/S1631-0713(03)00006-3.

Csontos, L., Vörös, A., 2004. Mesozoic plate tectonic reconstruction of the Carpathian region. Palaeogeogr. Palaeoclimatol. Palaeoecol. 210 (1), 1–56. https://doi.org/10.1016/j.palaeo.2004.02.033.

Davies, J.H.F.L., Marzoli, A., Bertrand, H., Youbi, N., Ernesto, M., Schaltegger, U., 2017. End-Triassic mass extinction started by intrusive CAMP activity. Nat. Commun. 8, 15596. https://doi.org/10.1038/ncomms15596.

de Lacerda, L.D., Turcq, B., Sifeddine, A., Cordeiro, R.C., 2017. Mercury accumulation rates in Caço Lake, NE Brazil during the past 20.000 years. J. S. Am. Earth Sci. 77, 42–50. https://doi.org/10.1016/j.jsames.2017.04.008.

Deenen, M.H.L., Ruhl, M., Bonis, N.R., Krijgsman, W., Kuerschner, W.M., Reitsma, M., van Bergen, M.J., 2010. A new chronology for the end-Triassic mass extinction. Earth Planet. Sci. Lett. 291 (1), 113–125. https://doi.org/10.1016/j.epsl.2010.01.003.

Dunham, G.E., DeWall, R.A., Senior, C.L., 2003. Fixed-bed studies of the interactions between mercury and coal combustion fly ash. Fuel Process. Technol. 82 (2), 197–213. https://doi.org/10.1016/S0378-3820(03)00070-5.

El Ghilani, S., Youbi, N., Madeira, J., Chellai, E.H., López-Galindo, A., Martins, L., Mata, J., 2017. Environmental implication of subaqueous lava flows from a continental Large Igneous Province: Examples from the Moroccan Central Atlantic Magmatic Province (CAMP). J. Afr. Earth Sci. 127, 211–221. https://doi.org/10.1016/j.jafrearsci.2016.07.021.

Fujisaki, W., Matsui, Y., Asanuma, H., Sawaki, Y., Suzuki, K., Maruyama, S., 2018. Global perturbations of carbon cycle during the Triassic–Jurassic transition recorded in the mid-Panthalassa. Earth Planet. Sci. Lett. 500, 105–116. https://doi.org/10.1016/j.epsl.2018.07.026.

Gehrke, G.E., Blum, J.D., Meyers, P.A., 2009. The geochemical behavior and isotopic composition of Hg in a mid-Pleistocene western Mediterranean sapropel. Geochim. Cosmochim. Acta 73 (6), 1651–1665. https://doi.org/10.1016/j.gca.2008.12.012.

Gill, G.A., Fitzgerald, W.F., 1988. Vertical mercury distributions in the oceans. Geochim. Cosmochim. Acta 52 (6), 1719–1728. https://doi.org/10.1016/0016-7037(88)90240-2.

Girginova, P.I., Daniel-da-Silva, A.L., Lopes, C.B., Figueira, P., Otero, M., Amaral, V.S., Pereira, E., Trindade, T., 2010. Silica coated magnetite particles for magnetic removal of Hg2+ from water. J. Colloid Interface Sci. 345 (2), 234–240. https://doi.org/10.1016/j.jcis.2010.01.087.

Götz, A.E., Ruckwied, K., Pálfy, J., Haas, J., 2009. Palynological evidence of synchronous changes within the terrestrial and marine realm at the Triassic/Jurassic boundary (Csővár section, Hungary). Rev. Palaeobot. Palynol. 156 (3), 401–409. https://doi.org/10.1016/j.revpalbo.2009.04.002.

Grasby, S.E., Sanei, H., Beauchamp, B., Chen, Z., 2013. Mercury deposition through the Permo–Triassic Biotic Crisis. Chem. Geol. 351, 209–216. https://doi.org/10.1016/j.chemgeo.2013.05.022.

Grasby, S.E., Beauchamp, B., Bond, D.P.G., Wignall, P.B., Sanei, H., 2015. Mercury anomalies associated with three extinction events (Capitanian Crisis, Latest Permian Extinction and the Smithian/Spathian Extinction) in NW Pangea. Geol. Mag. 153 (2), 285–297. https://doi.org/10.1017/S0016756815000436.

Grasby, S.E., Shen, W., Yin, R., Gleason, J.D., Blum, J.D., Lepak, R.F., Hurley, J.P., Beauchamp, B., 2017. Isotopic signatures of mercury contamination in latest Permian oceans. Geology 45 (1), 55–58. https://doi.org/10.1130/g38487.1.

Grasby, S.E., Them, T.R., Chen, Z., Yin, R., Ardakani, O.H., 2019. Mercury as a proxy for volcanic emissions in the geologic record. Earth Sci. Rev. 196, 102880. https://doi.org/10.1016/j.earscirev.2019.102880.

Guex, J., Bartolini, A., Atudorei, V., Taylor, D., 2004. High-resolution ammonite and carbon isotope stratigraphy across the Triassic–Jurassic boundary at New York Canyon (Nevada). Earth Planet. Sci. Lett. 225 (1), 29–41. https://doi.org/10.1016/j.epsl.2004.06.006.

Haas, J., Tardy-Filácz, E., 2004. Facies changes in the Triassic–Jurassic boundary interval in an intraplatform basin succession at Csővár (Transdanubian Range, Hungary). Sediment. Geol. 168 (1), 19–48. https://doi.org/10.1016/j.sedgeo.2004.03.002.

Haas, J., Tardy-Filácz, E., Oravecz-Scheffer, A., Góczán, F., Dosztály, L., 1997. Stratigraphy and sedimentology of an Upper Triassic toe-of-slope and basin

succession at Csővár, Hungary. Acta Geol. Hung. 40 (2), 111–177.
Haas, J., Götz, A.E., Pálfy, J., 2010. Late Triassic to Early Jurassic palaeogeography and eustatic history in the NW Tethyan realm: New insights from sedimentary and organic facies of the Csővár Basin (Hungary). Palaeogeogr. Palaeoclimatol. Palaeoecol. 291 (3), 456–468. https://doi.org/10.1016/j.palaeo.2010.03.014.
Haas, J., Hámor, G., Jámbor, Á., Kovács, S., Nagymarosy, A., Szederkényi, T., 2012. Geology of Hungary. Regional Geology Reviews. Springer-Verlag, Berlin Heidelberg. https://doi.org/10.1007/978-3-642-21910-8_3.
Haas, J., Jovanović, D., Görög, Á., Sudar, M.N., Józsa, S., Ozsvárt, P., Pelikán, P., 2019. Upper Triassic–Middle Jurassic resedimented toe-of-slope and hemipelagic basin deposits in the Dinaridic Ophiolite Belt, Zlatar Mountain, SW Serbia. Facies 65 (2), 23. https://doi.org/10.1007/s10347-019-0566-3.
Hachimi, H.E., Youbi, N., Madeira, J., Bensalah, M.K., Martins, L., Mata, J., Medina, F., Bertrand, H., Marzoli, A., Munhá, J., Bellieni, G., Mahmoudi, A., Abbou, M.B., Assafar, H., 2011. Morphology, internal architecture and emplacement mechanisms of lava flows from the Central Atlantic Magmatic Province (CAMP) of Argana Basin (Morocco). Geol. Soc. Lond., Spec. Publ. 357 (1), 167–193. https://doi.org/10.1144/sp357.9.
Hall, B., 1995. The gas phase oxidation of elemental mercury by ozone. Water Air Soil Pollut. 80 (1), 301–315. https://doi.org/10.1007/bf01189680.
Hall, G.E.M., Pelchat, P., 1997. Evaluation of a direct solid sampling atomic absorption spectrometer for the trace determination of mercury in geological samples. Analyst 122 (9), 921–924. https://doi.org/10.1039/A700194K.
Heimdal, T.H., Svensen, H.H., Ramezani, J., Iyer, K., Pereira, E., Rodrigues, R., Jones, M.T., Callegaro, S., 2018. Large-scale sill emplacement in Brazil as a trigger for the end-Triassic crisis. Sci. Rep. 8 (1), 141. https://doi.org/10.1038/s41598-017-18629-8.
Heimdal, T.H., Callegaro, S., Svensen, H.H., Jones, M.T., Pereira, E., Planke, S., 2019. Evidence for magma–evaporite interactions during the emplacement of the Central Atlantic Magmatic Province (CAMP) in Brazil. Earth Planet. Sci. Lett. 506, 476–492. https://doi.org/10.1016/j.epsl.2018.11.018.
Hesselbo, S.P., Robinson, S.A., Surlyk, F., Piasecki, S., 2002. Terrestrial and marine extinction at the Triassic-Jurassic boundary synchronized with major carbon-cycle perturbation: a link to initiation of massive volcanism? Geology 30 (3), 251–254. https://doi.org/10.1130/0091-7613(2002)030<0251:tameat>2.0.co;2.
Hesselbo, S.P., Korte, C., Ullmann, C.V., Ebbesen, A.L., 2020. Carbon and oxygen isotope records from the southern Eurasian Seaway following the Triassic-Jurassic boundary: Parallel long-term enhanced carbon burial and seawater warming. Earth-Sci. Rev. 103131. https://doi.org/10.1016/j.earscirev.2020.103131.
Hillebrandt, A.V., Krystyn, L., Kürschner, W.M., Bonis, N.R., Ruhl, M., Richoz, S., Schobben, M.A.N., Urlichs, M., Bown, P.R., Kment, K., McRoberts, C.A., Simms, M., Tomašových, A., 2013. The Global Stratotype Sections and Point (GSSP) for the base of the Jurassic System at Kuhjoch (Karwendel Mountains, Northern Calcareous Alps, Tyrol, Austria). Episodes 36 (3), 162–198. https://doi.org/10.18814/epiiugs/2013/v36i3/001.
Holmes, C.D., Jacob, D.J., Corbitt, E.S., Mao, J., Yang, X., Talbot, R., Slemr, F., 2010. Global atmospheric model for mercury including oxidation by bromine atoms. Atmos. Chem. Phys. 10 (24), 12037–12057. https://doi.org/10.5194/acp-10-12037-2010.
Hüsing, S.K., Beniest, A., van der Boon, A., Abels, H.A., Deenen, M.H.L., Ruhl, M., Krijgsman, W., 2014. Astronomically-calibrated magnetostratigraphy of the Lower Jurassic marine successions at St. Audrie's Bay and East Quantoxhead (Hettangian–Sinemurian; Somerset, UK). Palaeogeogr. Palaeoclimatol. Palaeoecol. 403, 43–56. https://doi.org/10.1016/j.palaeo.2014.03.022.
Jaraula, C.M.B., Grice, K., Twitchett, R.J., Böttcher, M.E., LeMetayer, P., Dastidar, A.G., Opazo, L.F., 2013. Elevated pCO_2 leading to Late Triassic extinction, persistent photic zone euxinia, and rising sea levels. Geology 41 (9), 955–958. https://doi.org/10.1130/g34183.1.
Jones, M.T., Percival, L.M.E., Stokke, E.W., Frieling, J., Mather, T.A., Riber, L., Schubert, B.A., Schultz, B., Tegner, C., Planke, S., Svensen, H.H., 2019. Mercury anomalies across the Palaeocene-Eocene Thermal Maximum. Clim. Past Discuss. 2018, 1–35. https://doi.org/10.5194/cp-2018-121.
Karádi, V., 2018. Upper Triassic conodonts from the Csővár area and the Buda Hills, Hungary and their geological applications. Eötvös Loránd University, pp. 120 PhD thesis.
Karádi, V., Cau, A., Mazza, M., Rigo, M., 2019. The last phase of conodont evolution during the Late Triassic: Integrating biostratigraphic and phylogenetic approaches. Palaeogeogr. Palaeoclimatol. Palaeoecol. https://doi.org/10.1016/j.palaeo.2019.03.045.
Korte, C., Kozur, H.W., 2011. Bio-and chemostratigraphic assessment of carbon isotope records across the Triassic–Jurassic boundary at Csővár quarry (Hungary) and Kendlbachgraben (Austria) and implications for global correlations. Bull. Geol. Soc. Den. 59, 101–115.
Korte, C., Thibault, N., Ullmann, C.V., Clémence, M.-E., Mette, W., Olsen, T.K., Rizzi, M., Ruhl, M., 2017. Brachiopod biogeochemistry and isotope stratigraphy from the Rhaetian Eiberg section in Austria: potentials and limitations. N. Jb. Geol. Paläont. (Abh.) 284 (2), 117–138. https://doi.org/10.1127/njgpa/2017/0651.
Korte, C., Ruhl, M., Pálfy, J., Ullmann, C.V., Hesselbo, S.P., 2019. Chemostratigraphy across the Triassic–Jurassic boundary. In: Sial, A.N., Gaucher, C., Ramkumar, M., Ferreira, V.P. (Eds.), Chemostratigraphy Across Major Chronological Boundaries. AGU Geophysical Monograph Seriespp. 185–210. https://doi.org/10.1002/9781119382508.ch10.
Kozur, H., 1993. First evidence of Liassic in the vicinity of Csővár (Hungary), and its paleogeographic and paleotectonic significance. Jahrb. Geol. Bundesanst. 136 (1), 89–98.
Kozur, H., Mock, R., 1991. New Middle Carnian and Rhaetian conodonts from Hungary and the Alps. Stratigraphic importance and tectonic implications for the Buda Mountains and adjacent areas. Jahrb. Geol. Bundesanst. 134 (2), 271–297.
Kozur, H., Mostler, H., 1990. Saturnaliacae Deflandre and some other stratigraphically important Radiolaria from the Hettangian of Lenggries/Isar (Bavaria/Northern Calcareous Alps). Geologisch-Paläontologische Mitteilungen 17, 179–248.
Landis, G.P., 1983. Harding Iceland spar: A new δ18O − δ13C carbonate standard for hydrothermal minerals. Chem. Geol. 41, 91–94. https://doi.org/10.1016/S0009-2541(83)80008-4.
Li, L., Wang, Y., Kürschner, W.M., Ruhl, M., Vajda, V., 2020. Palaeovegetation and palaeoclimate changes across the Triassic–Jurassic transition in the Sichuan Basin, China. Palaeogeogr. Palaeoclimatol. Palaeoecol. https://doi.org/10.1016/j.palaeo.2020.109891. 109891.
Lindström, S., van de Schootbrugge, B., Dybkjær, K., Pedersen, G.K., Fiebig, J., Nielsen, L.H., Richoz, S., 2012. No causal link between terrestrial ecosystem change and methane release during the end-Triassic mass extinction. Geology 40 (6), 531–534. https://doi.org/10.1130/g32928.1.
Lindström, S., van de Schootbrugge, B., Hansen, K.H., Pedersen, G.K., Alsen, P., Thibault, N., Dybkjær, K., Bjerrum, C.J., Nielsen, L.H., 2017. A new correlation of Triassic–Jurassic boundary successions in NW Europe, Nevada and Peru, and the Central Atlantic Magmatic Province: a time-line for the end-Triassic mass extinction. Palaeogeogr. Palaeoclimatol. Palaeoecol. 478, 80–102. https://doi.org/10.1016/j.palaeo.2016.12.025.
Lindström, S., Sanei, H., van de Schootbrugge, B., Pedersen, G.K., Lesher, C.E., Tegner, C., Heunisch, C., Dybkjær, K., Outridge, P.M., 2019. Volcanic mercury and mutagenesis in land plants during the end-Triassic mass extinction. Sci. Adv. 5 (10). https://doi.org/10.1126/sciadv.aaw4018. eaaw4018.
Lucas, S.G., Taylor, D.G., Guex, J., Tanner, L.H., Krainer, K., 2007. The proposed global stratotype section and point for the base of the Jurassic System in the New York Canyon area, Nevada, USA. In: Lucas, S.G., Spielmann, J.A. (Eds.), Triassic of the American West. New Mexico Museum of Natural History and Science Bulletin. New Mexico Museum of Natural History and Science Albuquerque, vol. 40. pp. 139–168.
Mander, L., Kürschner, W.M., McElwain, J.C., 2013. Palynostratigraphy and vegetation history of the Triassic–Jurassic transition in East Greenland. J. Geol. Soc. 170 (1), 37–46. https://doi.org/10.1144/jgs2012-018.
Marzoli, A., Renne, P.R., Piccirillo, E.M., Ernesto, M., Bellieni, G., Min, A.D., 1999. Extensive 200-Million-year-old continental flood basalts of the Central Atlantic magmatic province. Science 284 (5414), 616–618. https://doi.org/10.1126/science.284.5414.616.
Marzoli, A., Bertrand, H., Knight, K.B., Cirilli, S., Buratti, N., Vérati, C.l., Nomade, S.b., Renne, P.R., Youbi, N., Martini, R., Allenbach, K., Neuwerth, R., Rapaille, C.d., Zaninetti, L., Bellieni, G., 2004. Synchrony of the Central Atlantic magmatic province and the Triassic-Jurassic boundary climatic and biotic crisis. Geology 32 (11), 973–976. https://doi.org/10.1130/g20652.1.
Marzoli, A., Bertrand, H., Youbi, N., Callegaro, S., Merle, R., Reisberg, L., Chiaradia, M., Brownlee, S.I., Jourdan, F., Zanetti, A., Davies, J.H.F.L., Cuppone, T., Mahmoudi, A., Medina, F., Renne, P.R., Bellieni, G., Crivellari, S., El Hachimi, H., Bensalah, M.K., Meyzen, C.M., Tegner, C., 2019. The Central Atlantic Magmatic Province (CAMP) in Morocco. J. Petrol. 60 (5), 945–996. https://doi.org/10.1093/petrology/egz021.
McElwain, J.C., Chaloner, W.G., 1995. Stomatal density and index of fossil plants track atmospheric carbon dioxide in the palaeozoic. Ann. Bot. 76 (4), 389–395. https://doi.org/10.1006/anbo.1995.1112.
McElwain, J.C., Beerling, D.J., Woodward, F.I., 1999. Fossil plants and global warming at the Triassic-jurassic boundary. Science 285 (5432), 1386–1390. https://doi.org/10.1126/science.285.5432.1386.
Melamed, R., da Luz, A.B., 2006. Efficiency of industrial minerals on the removal of mercury species from liquid effluents. Sci. Total Environ. 368 (1), 403–406. https://doi.org/10.1016/j.scitotenv.2005.09.091.
Mette, W., Elsler, A., Korte, C., 2012. Palaeoenvironmental changes in the Late Triassic (Rhaetian) of the Northern Calcareous Alps: clues from stable isotopes and microfossils. Palaeogeogr. Palaeoclimatol. Palaeoecol. 350-352, 62–72. https://doi.org/10.1016/j.palaeo.2012.06.013.
Mette, W., Clemence, M.-E., Thibault, N., Korte, C., Konrad, B., Ullmann, C.V., 2019. Sedimentology, carbon isotope stratigraphy and micropalaeontology of the Rhaetian Zlambach Formation– Implications for the Dachstein carbonate platform development (Northern Calcareous Alps, Austria). Sediment. Geol. 382, 47–60. https://doi.org/10.1016/j.sedgeo.2018.12.009.
Olsen, P.E., Kent, D.V., Sues, H.-D., Koeberl, C., Huber, H., Montanari, A., Rainforth, E.C., Fowell, S.J., Szajna, M.J., Hartline, B.W., 2002. Ascent of dinosaurs linked to an iridium anomaly at the Triassic-Jurassic boundary. Science 296 (5571), 1305–1307. https://doi.org/10.1126/science.1065522.
Outridge, H. Sanei, Stern, Hamilton, Goodarzi, F., 2007. Evidence for control of mercury accumulation rates in Canadian high arctic lake sediments by variations of aquatic primary productivity. Environ. Sci. Technol. 41 (15), 5259–5265. https://doi.org/10.1021/es070408x.
Pálfy, J., 2003. Volcanism of the Central Atlantic Magmatic Province as a potential driving force in the end-Triassic mass extinction. Washington DC Am. Geophys. Union Geophys. Monogr. Ser. 136, 255–267. https://doi.org/10.1029/136GM014.
Pálfy, J., Dosztály, L., 2000. A new marine Triassic-Jurassic boundary section in Hungary: preliminary results. In: Hall, R.L., Smith, P.L. (Eds.), Advances in Jurassic Research 2000. GeoResearch Forum. TransTech Publications, Zurich, pp. 173–179.
Pálfy, J., Kocsis, Á.T., 2014. Volcanism of the Central Atlantic Magmatic Province as the trigger of environmental and biotic changes around the Triassic-Jurassic boundary. In: Keller, G., Kerr, A.C. (Eds.), Volcanism, Impacts and Mass Extinctions: Causes and Effects. Geological Society of America Special Paper, Boulder, CO, pp. 245–261. https://doi.org/10.1130/2014.2505(12).
Pálfy, J., Zajzon, N., 2012. Environmental changes across the Triassic–Jurassic boundary and coeval volcanism inferred from elemental geochemistry and mineralogy in the

Kendlbachgraben section (Northern Calcareous Alps, Austria). Earth Planet. Sci. Lett. 335-336, 121–134. https://doi.org/10.1016/j.epsl.2012.01.039.
Pálfy, J., Mortensen, J.K., Carter, E.S., Smith, P.L., Friedman, R.M., Tipper, H.W., 2000. Timing the end-Triassic mass extinction: first on land, then in the sea? Geology 28 (1), 39–42. https://doi.org/10.1130/0091-7613(2000)28<39:ttemef>2.0.co;2.
Pálfy, J., Demény, A., Haas, J., Hetényi, M., Orchard, M., Vető, I., 2001. Carbon isotope anomaly and other geochemical changes at the Triassic-Jurassic boundary from a marine section in Hungary. Geology 29 (11), 1047–1050. https://doi.org/10.1130/0091-7613(2001)029<1047:CIAAOG>2.0.CO;2.
Pálfy, J., Smith, P.L., Mortensen, J.K., 2002. Dating the end-Triassic and Early Jurassic mass extinctions, correlative large igneous provinces, and isotopic events. In: Koeberl, C., Macleod, K.G. (Eds.), Catastrophic Events and Mass Extinctions: Impacts and Beyond. Geological Society of America Special Paper, vol. 356. pp. 523–532. https://doi.org/10.1130/0-8137-2356-6.523.
Pálfy, J., Demény, A., Haas, J., Carter, E.S., Görög, Á., Halász, D., Oravecz-Scheffer, A., Hetényi, M., Márton, E., Orchard, M.J., Ozsvárt, P., Vető, I., Zajzon, N., 2007. Triassic-Jurassic boundary events inferred from integrated stratigraphy of the Csővár section, Hungary. Palaeogeogr. Palaeoclimatol. Palaeoecol. 244 (1-4), 11–33. https://doi.org/10.1016/j.palaeo.2006.06.021.
Panfili, G., Cirilli, S., Corso, J.D., Bertrand, H., Medina, F., Youbi, N., Marzoli, A., 2019. New biostratigraphic constraints show rapid emplacement of the Central Atlantic Magmatic Province (CAMP) during the end-Triassic mass extinction interval. Glob. Planet. Chang. 172, 60–68. https://doi.org/10.1016/j.gloplacha.2018.09.009.
Pederson, C.L., McNeill, D.F., Klaus, J.S., Swart, P.K., 2015. Deposition and diagenesis of marine oncoids: implications for development of carbonate porosity. J. Sediment. Res. 85 (11), 1323–1333. https://doi.org/10.2110/jsr.2015.77.
Percival, L.M.E., Witt, M.L.I., Mather, T.A., Hermoso, M., Jenkyns, H.C., Hesselbo, S.P., Al-Suwaidi, A.H., Storm, M.S., Xu, W., Ruhl, M., 2015. Globally enhanced mercury deposition during the end-Pliensbachian extinction and Toarcian OAE: A link to the Karoo–Ferrar Large Igneous Province. Earth Planet. Sci. Lett. 428, 267–280. https://doi.org/10.1016/j.epsl.2015.06.064.
Percival, L.M.E., Ruhl, M., Hesselbo, S.P., Jenkyns, H.C., Mather, T.A., Whiteside, J.H., 2017. Mercury evidence for pulsed volcanism during the end-Triassic mass extinction. Proc. Natl. Acad. Sci. 114 (30), 7929–7934. https://doi.org/10.1073/pnas.1705378114.
Percival, L.M.E., Jenkyns, H.C., Mather, T.A., Dickson, A.J., Batenburg, S.J., Ruhl, M., Hesselbo, S.P., Barclay, R., Jarvis, I., Robinson, S.A., Woelders, L., 2018. Does large igneous province volcanism always perturb the mercury cycle? Comparing the records of Oceanic Anoxic Event 2 and the end-Cretaceous to other Mesozoic events. Am. J. Sci. 318 (8), 799–860. https://doi.org/10.2475/08.2018.01.
Poissant, L., 1997. Field observations of total gaseous mercury behaviour: interactions with ozone concentration and water vapour mixing ratio in air at a rural site. Water Air Soil Pollut. 97 (3), 341–353. https://doi.org/10.1007/bf02407471.
Pyle, D.M., Mather, T.A., 2003. The importance of volcanic emissions for the global atmospheric mercury cycle. Atmos. Environ. 37 (36), 5115–5124. https://doi.org/10.1016/j.atmosenv.2003.07.011.
Ravichandran, M., 2004. Interactions between mercury and dissolved organic matter—a review. Chemosphere 55 (3), 319–331. https://doi.org/10.1016/j.chemosphere.2003.11.011.
Riccardi, A.C., 2019. Cephalopods from the Triassic-Jurassic boundary interval in west central Argentina. N. Jb. Geol. Paläont. (Abh.) 291 (2), 135–157. https://doi.org/10.1127/njgpa/2019/0778.
Rizzi, M., Thibault, N., Ullmann, C.V., Ruhl, M., Olsen, T.K., Moreau, J., Clémence, M.-E., Mette, W., Korte, C., 2020. Sedimentology and carbon isotope stratigraphy of the Rhaetian Hochalm section (Late Triassic, Austria). Glob. Planet. Chang. 191, 103210. https://doi.org/10.1016/j.gloplacha.2020.103210.
Ruhl, M., Kürschner, W.M., 2011. Multiple phases of carbon cycle disturbance from large igneous province formation at the Triassic-Jurassic transition. Geology 39 (5), 431–434. https://doi.org/10.1130/g31680.1.
Ruhl, M., Kürschner, W.M., Krystyn, L., 2009. Triassic–Jurassic organic carbon isotope stratigraphy of key sections in the western Tethys realm (Austria). Earth Planet. Sci. Lett. 281 (3), 169–187. https://doi.org/10.1016/j.epsl.2009.02.020.
Ruhl, M., Veld, H., Kürschner, W.M., 2010a. Sedimentary organic matter characterization of the Triassic–Jurassic boundary GSSP at Kuhjoch (Austria). Earth Planet. Sci. Lett. 292 (1), 17–26. https://doi.org/10.1016/j.epsl.2009.12.046.
Ruhl, M., Deenen, M.H.L., Abels, H.A., Bonis, N.R., Krijgsman, W., Kürschner, W.M., 2010b. Astronomical constraints on the duration of the early Jurassic Hettangian stage and recovery rates following the end-Triassic mass extinction (St Audrie's Bay/East Quantoxhead, UK). Earth Planet. Sci. Lett. 295 (1), 262–276. https://doi.org/10.1016/j.epsl.2010.04.008.
Ruhl, M., Bonis, N.R., Reichart, G.-J., Damsté, J.S.S., Kürschner, W.M., 2011. Atmospheric carbon injection linked to end-triassic mass extinction. Science 333 (6041), 430–434. https://doi.org/10.1126/science.1204255.
Ruhl, M., Hesselbo, S.P., Al-Suwaidi, A., Jenkyns, H.C., Damborenea, S.E., Manceñido, M.O., Storm, M., Mather, T.A., Riccardi, A.C., 2020. On the onset of Central Atlantic Magmatic Province (CAMP) volcanism and environmental and carbon-cycle change at the Triassic–Jurassic transition (Neuquén Basin, Argentina). Earth Sci. Rev. 103229. https://doi.org/10.1016/j.earscirev.2020.103229.
Sanei, H., Grasby, S.E., Beauchamp, B., 2012. Latest Permian mercury anomalies. Geology 40 (1), 63–66. https://doi.org/10.1130/G32596.1.
Scaife, J.D., Ruhl, M., Dickson, A.J., Mather, T.A., Jenkyns, H.C., Percival, L.M.E., Hesselbo, S.P., Cartwright, J., Eldrett, J.S., Bergman, S.C., Minisini, D., 2017. Sedimentary Mercury Enrichments as a Marker for Submarine Large Igneous Province Volcanism? Evidence From the Mid-Cenomanian Event and Oceanic Anoxic Event 2 (Late Cretaceous). Geochem. Geophys. Geosyst. 18 (12), 4253–4275. https://doi.org/10.1002/2017GC007153.
Schoene, B., Eddy, M.P., Samperton, K.M., Keller, C.B., Keller, G., Adatte, T., Khadri, S.F.R., 2019. U-Pb constraints on pulsed eruption of the Deccan Traps across the end-Cretaceous mass extinction. Science 363 (6429), 862–866. https://doi.org/10.1126/science.aau2422.
Schroeder, W.H., Munthe, J., 1998. Atmospheric mercury—An overview. Atmos. Environ. 32 (5), 809–822. https://doi.org/10.1016/S1352-2310(97)00293-8.
Self, S., Widdowson, M., Thordarson, T., Jay, A.E., 2006. Volatile fluxes during flood basalt eruptions and potential effects on the global environment: a Deccan perspective. Earth Planet. Sci. Lett. 248 (1), 518–532. https://doi.org/10.1016/j.epsl.2006.05.041.
Self, S., Schmidt, A., Mather, T., 2014. Emplacement characteristics, time scales, and volcanic gas release rates of continental flood basalt eruptions on Earth. Geol. Soc. Am. Spec. Pap. 505, 319–337. https://doi.org/10.1130/2014.2505(16).
Selin, N.E., 2009. Global Biogeochemical Cycling of Mercury: A Review. Annu. Rev. Environ. Resour. 34 (1), 43–63. https://doi.org/10.1146/annurev.environ.051308.084314.
Shen, J., Algeo, T.J., Chen, J., Planavsky, N.J., Feng, Q., Yu, J., Liu, J., 2019a. Mercury in marine Ordovician/Silurian boundary sections of South China is sulfide-hosted and non-volcanic in origin. Earth Planet. Sci. Lett. 511, 130–140. https://doi.org/10.1016/j.epsl.2019.01.028.
Shen, J., Algeo, T.J., Planavsky, N.J., Yu, J., Feng, Q., Song, H., Song, H., Rowe, H., Zhou, L., Chen, J., 2019b. Mercury enrichments provide evidence of Early Triassic volcanism following the end-Permian mass extinction. Earth Sci. Rev. 195, 191–212. https://doi.org/10.1016/j.earscirev.2019.05.010.
Shen, J., Feng, Q., Algeo, T.J., Liu, J., Zhou, C., Wei, W., Liu, J., Them, T.R., Gill, B.C., Chen, J., 2020. Sedimentary host phases of mercury (Hg) and implications for use of Hg as a volcanic proxy. Earth Planet. Sci. Lett. 543, 116333. https://doi.org/10.1016/j.epsl.2020.116333.
Spötl, C., Vennemann, T.W., 2003. Continuous-flow isotope ratio mass spectrometric analysis of carbonate minerals. Rapid Commun. Mass Spectrom. 17 (9), 1004–1006. https://doi.org/10.1002/rcm.1010.
Steinthorsdottir, M., Jeram, A.J., McElwain, J.C., 2011. Extremely elevated CO2 concentrations at the Triassic/Jurassic boundary. Palaeogeogr. Palaeoclimatol. Palaeoecol. 308 (3), 418–432. https://doi.org/10.1016/j.palaeo.2011.05.050.
Storm, M.S., Hesselbo, S.P., Jenkyns, H.C., Ruhl, M., Ullmann, C.V., Xu, W., Leng, M.J., Riding, J.B., Gorbanenko, O., 2020. Orbital pacing and secular evolution of the Early Jurassic carbon cycle. Proc. Natl. Acad. Sci. https://doi.org/10.1073/pnas.1912094117. 201912094.
Swift, A., 1995. A review of the nature and outcrop of the 'White Lias' facies of the Langport Member (Penarth Group: Upper Triassic) in Britain. Proc. Geol. Assoc. 106, 247–258.
Szabó, J., 1860. Geologische Detailkonte des Grensgebietes des Nograder und Pesther Comitates. Jahrbuch des kaiserlich-königlichen geologischen Reichanstalt, Sitzungberichte, pp. 41–44.
Thibodeau, A.M., Ritterbush, K., Yager, J.A., West, A.J., Ibarra, Y., Bottjer, D.J., Berelson, W.M., Bergquist, B.A., Corsetti, F.A., 2016. Mercury anomalies and the timing of biotic recovery following the end-Triassic mass extinction. Nat. Commun. 7, 11147. https://doi.org/10.1038/ncomms11147.
van de Schootbrugge, B., Quan, T.M., Lindström, S., Püttmann, W., Heunisch, C., Pross, J., Fiebig, J., Petschick, R., Röhling, H.G., Richoz, S., Rosenthal, Y., Falkowski, P.G., 2009. Floral changes across the Triassic/Jurassic boundary linked to flood basalt volcanism. Nat. Geosci. 2 (8), 589–594. https://doi.org/10.1038/ngeo577.
Veizer, J., Ala, D., Azmy, K., Bruckschen, P., Buhl, D., Bruhn, F., Carden, G.A.F., Diener, A., Ebneth, S., Godderis, Y., Jasper, T., Korte, C., Pawellek, F., Podlaha, O.G., Strauss, H., 1999. $^{87}Sr/^{86}Sr$, $\delta^{13}C$ and $\delta^{18}O$ evolution of Phanerozoic seawater. Chem. Geol. 161 (1–3), 59–88. https://doi.org/10.1016/S0009-2541(99)00081-9.
Wang, X., Cawood, P.A., Zhao, H., Zhao, L., Grasby, S.E., Chen, Z.-Q., Zhang, L., 2019. Global mercury cycle during the end-Permian mass extinction and subsequent Early Triassic recovery. Earth Planet. Sci. Lett. 513, 144–155. https://doi.org/10.1016/j.epsl.2019.02.026.
Ward, P.D., Haggart, J.W., Carter, E.S., Wilbur, D., Tipper, H.W., Evans, T., 2001. Sudden productivity collapse associated with the triassic-Jurassic boundary mass extinction. Science 292 (5519), 1148–1151. https://doi.org/10.1126/science.1058574.
Ward, P.D., Garrison, G.H., Williford, K.H., Kring, D.A., Goodwin, D., Beattie, M.J., McRoberts, C.A., 2007. The organic carbon isotopic and paleontological record across the Triassic–Jurassic boundary at the candidate GSSP section at Ferguson Hill, Muller Canyon, Nevada, USA. Palaeogeogr. Palaeoclimatol. Palaeoecol. 244 (1), 281–289. https://doi.org/10.1016/j.palaeo.2006.06.042.
Waters, C.N., Zalasiewicz, J., Summerhayes, C., Barnosky, A.D., Poirier, C., Gałuszka, A., Cearreta, A., Edgeworth, M., Ellis, E.C., Ellis, M., Jeandel, C., Leinfelder, R., McNeill, J.R., Richter, D.D., Steffen, W., Syvitski, J., Vidas, D., Wagreich, M., Williams, M., Zhisheng, A., Grinevald, J., Odada, E., Oreskes, N., Wolfe, A.P., 2016. The Anthropocene is functionally and stratigraphically distinct from the Holocene. Science 351 (6269). https://doi.org/10.1126/science.aad2622. aad2622.
Weedon, G.P., Page, K.N., Jenkyns, H.C., 2019. Cyclostratigraphy, stratigraphic gaps and the duration of the Hettangian Stage (Jurassic): insights from the Blue Lias Formation of southern Britain. Geol. Mag. 156 (9), 1469–1509. https://doi.org/10.1017/S0016756818000808.
Whiteside, J.H., Olsen, P.E., Kent, D.V., Fowell, S.J., Et-Touhami, M., 2007. Synchrony between the Central Atlantic magmatic province and the Triassic–Jurassic mass-extinction event? Palaeogeogr. Palaeoclimatol. Palaeoecol. 244 (1), 345–367. https://doi.org/10.1016/j.palaeo.2006.06.035.
Wignall, P.B., 2001. Large igneous provinces and mass extinctions. Earth Sci. Rev. 53 (1), 1–33. https://doi.org/10.1016/S0012-8252(00)00037-4.
Wignall, P., 2005. The link between large igneous province eruptions and mass extinctions. Elements 1 (5), 293–297. https://doi.org/10.2113/gselements.1.5.293.

Xu, W., Ruhl, M., Hesselbo, S.P., Riding, J.B., Jenkyns, H.C., 2017. Orbital pacing of the Early Jurassic carbon cycle, black-shale formation and seabed methane seepage. Sedimentology 64 (1), 127–149. https://doi.org/10.1111/sed.12329.

Yang, J., Zhao, Y., Zhang, J., Zheng, C., 2014. Regenerable cobalt oxide loaded magnetosphere catalyst from fly ash for mercury removal in coal combustion flue gas. Environ. Sci. Technol. 48 (24), 14837–14843. https://doi.org/10.1021/es504419v.

Yang, J., Zhao, Y., Zhang, S., Liu, H., Chang, L., Ma, S., Zhang, J., Zheng, C., 2017. Mercury removal from flue gas by magnetospheres present in fly ash: role of iron species and modification by HF. Fuel Process. Technol. 167, 263–270. https://doi.org/10.1016/j.fuproc.2017.07.016.

Zajzon, N., Kristály, F., Pálfy, J., Németh, T., 2012. Detailed clay mineralogy of the Triassic-Jurassic boundary section at Kendlbachgraben (Northern Calcareous Alps, Austria). Clay Miner. 47 (2), 177–189. https://doi.org/10.1180/claymin.2012.047.2.03.